AD NUMBER

ADB022461

LIMITATION CHANGES

TO:

Approved for public release; distribution is unlimited.

FROM:

Distribution authorized to U.S. Gov't. agencies only; Test and Evaluation; 20 OCT 1977. Other requests shall be referred to Space and Missile Systems Organization, Attn: RSMM, P.O. Box 92960.

AUTHORITY

SAMSO ltr, 16 Oct 1978

SAMSO-TR-77-50

BALLISTIC REENTRY VEHICLE AERODYNAMIC COEFFICIENT ESTIMATION USING AN ADVANCED SYSTEM IDENTIFICATION TECHNIQUE

SYSTEMS CONTROL, INC. (VT)
Palo Alto, California 94304

August 1977

Final Report for Period 1 March 1976-1 March 1977

Prepared for

SPACE AND MISSILE SYSTEMS ORGANIZATION
Los Angeles Air Force Station
P.O. Box 92960 Worldway Postal Center
Los Angeles, California 90009

APPROVAL STATEMENT

This final report was submitted by Systems Control, Inc (Vt), 1801 Page Mill Road, Palo Alto, California 94304, under Contract F04701-76-C-0127 with the Space and Missile Systems Organization, Los Angeles Air Force Station, P. O. Box 92960, Worldway Postal Center, Los Angeles, California 90009. Capt James A. Davis, RSMM, was the Systems Program Office Project Manager. Distribution of this report will be in accordance with the distribution statement on the cover and on the DD Form 1473.

This technical report has been reviewed and is approved for publication. The conclusions and findings contained herein do not necessarily represent an Air Force position.

FOR THE COMMANDER

DAVID C. HALL, 1Lt, USAF
Project Officer

FRAZIER J. HELLINGS, Lt Col, USAF
Chief, Maneuvering Vehicle Division

UNCLASSIFIED

SECURITY CLASSIFICATION OF THIS PAGE (When Data Entered)

REPORT DOCUMENTATION PAGE

READ INSTRUCTIONS BEFORE COMPLETING FORM

1. REPORT NUMBER	2. GOVT ACCESSION NO. Coefficient Estimation
	3. RECIPIENT'S CATALOG NUMBER
4. TITLE (and Subtitle) BALLISTIC REENTRY VEHICLE AERODYNAMIC ~~MODELING~~ USING AN ADVANCED SYSTEM IDENTIFICATION TECHNIQUE.	5. TYPE OF REPORT & PERIOD COVERED Final Report. 1 March 76 — 1 March 77
	6. PERFORMING ORG. REPORT NUMBER SCI-5412-002
7. AUTHOR(s) Narendra K. Gupta and W. Earl Hall, Jr	8. CONTRACT OR GRANT NUMBER(s) F04701-76-C-0127
9. PERFORMING ORGANIZATION NAME AND ADDRESS SYSTEMS CONTROL, INC. (Vt) 1801 Page Mill Road Palo Alto, CA. 94304	10. PROGRAM ELEMENT, PROJECT, TASK AREA & WORK UNIT NUMBERS
11. CONTROLLING OFFICE NAME AND ADDRESS SPACE AND MISSILE SYSTEMS ORGANIZATION (RSMM) P.O. Box 92960, Worldway Postal Center Los Angeles, CA. 90009	12. REPORT DATE August 1977
	13. NUMBER OF PAGES 95
14. MONITORING AGENCY NAME & ADDRESS (if different from Controlling Office) 12 96p.	15. SECURITY CLASS. (of this report) UNCLASSIFIED
	15a. DECLASSIFICATION/DOWNGRADING SCHEDULE

16. DISTRIBUTION STATEMENT (of this Report) T&E 20 OCT 1977

Distribution limited to U.S. Government agencies only. Other requests for this document must be referred to SAMSO/RSMM, P.O. Box 92960, Worldway Postal Center, Los Angeles, CA. 90009.

17. DISTRIBUTION STATEMENT (of the abstract entered in Block 20, if different from Report)

Unlimited. 18 SAMSO 19 TR-77-54

DDC RECEIVED OCT 20 1977 B

18. SUPPLEMENTARY NOTES

19. KEY WORDS (Continue on reverse side if necessary and identify by block number)

Ballistic Reentry Vehicle
Flight Testing
Aerodynamic Coefficient Estimation
Ballistic Reentry Vehicle Data Processing

20. ABSTRACT (Continue on reverse side if necessary and identify by block number)

This report develops post-flight data processing methods for aerodynamic coefficient estimation of ballistic reentry vehicles based on advanced system identification technology. This post-flight data processing involves reconstruction of unmeasured channels, aerodynamic coefficient model structure determination and maximum likelihood parameter estimation. The methods are verified on a simulation trajectory and on a flight test trajectory. It is shown that the techniques are general enough to handle a variety of regimes encountered by a typical ballistic reentry vehicle.

DD FORM 1 JAN 73 1473 EDITION OF 1 NOV 65 IS OBSOLETE

389 333

SECURITY CLASSIFICATION OF THIS PAGE (When Data Entered)

FOREWARD

This work was performed as one phase of Contract F04701-76-C-0127 on the development of advanced system identification techniques to reentry vehicle data processing. The technical monitor at SAMSO was Capt. James A. Davis and at The Aerospace Corporation was Mr. Robert Palmer. At Systems Control, Inc. (Vt), W. Earl Hall, Jr., managed the project and Narendra K. Gupta was the principal engineer. Project engineers were David Klinger and Robert Walker.

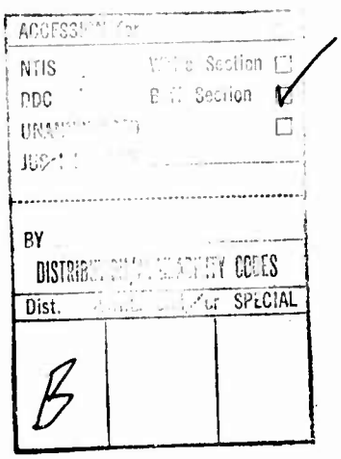

CONTENTS

CONTENTS (Continued)

LIST OF SYMBOLS

A_{cg}	Measured acceleration transferred to c.g. ($ft\ sec^{-2}$)
b	Characteristic length (ft)
B	Innovation covariance
C_b	Body fixed moment coefficient (nondimensional)
C_x, C_y, C_z	Force coefficients along x, y, and z axes (nondimensional)
C_{Z_c}	Out-of-plane moment (nondimensional)
C_m, C_n, C_ℓ	Moment coefficients about x, y, and z axes (nondimensional)
C_N'	In-plane moment coefficient (nondimensional)
C_Z	Out-of-plane moment coefficient (nondimensional)
C_{m_T}	Total moment coefficient (nondimensional)
F	Statistical F-ratio (nondimensional)
g	Acceleration due to gravity ($ft\ sec^{-2}$)
I	Moment of inertia about axis of symmetry ($slug\ ft^2$)
I_x	Moment of inertia about pitch axis ($slug\ ft^2$)
m	Mass (slug)
p,q,r	Roll, pitch and yaw rates ($rad\ sec^{-1}$)
q_s	Dynamic pressure ($slug\ ft^{-1}\ sec^{-2}$)
R	Multiple correlation coefficient
Re	Reynolds number
s	Characteristic surface area (ft^2)
u,v,w	Longitudinal, lateral and normal velocity components ($ft\ sec^{-1}$)
y(i), Y(i)	Measurements

LIST OF SYMBOLS (Continued)

X_A, Y_A, Z_A	Wind system axes
X_B, X_B, X_B	Body fixed system axes
α	Angle-of-attack (rad)
α_T	Total angle-of-attack (rad)
ϕ	Roll angle (rad)
ϕ_w	Windward meridian (rad)
ϕ_b	Roll orientation angle of plane where body fixed moment acts (rad)
ϕ_L	Angle between moment plane and round plane (rad)
θ	Pitch angle (rad)
θ	Vector of unknown parameters
ψ	Yaw angle (rad)
μ	Mach number (nondimensional)
ω	Angular velocity vector (rad sec^{-1})

CHAPTER I

INTRODUCTION AND SUMMARY

1.1 INTRODUCTION

The accuracy of advanced ballistic missile systems depends ultimately on the capability to compensate for trajectory errors encountered in boost, deployment and reentry phases. The error compensation procedures, however, depend on the extent to which system performance anomalies can be quantified in terms of guidance, navigation, or basic configuration parameters. This quantification is achieved most efficiently by development of a systematic mathematical modeling methodology.

The reentry phase represents a mission stage which is difficult to model. This is because of the complexity of the dynamic, aerodynamic, thermodynamic, and material phenomena, all of which affect the reentry body motion and, hence, accuracy. Development of the required modeling methodology is therefore a continuing effort of some technical sophistication. Many attempts, both theoretical and experimental, have been made to understand the flow field around a spinning ballistic reentry vehicle. Theoretical techniques are difficult to use for accurately modeling the aerodynamics because of the complex interaction of the many physical factors. Wind tunnel tests and analysis significantly contribute to understanding these factors, but are not yet able to provide sufficient data for many extreme regimes (e.g., high Reynolds number, high windward meridian rate and in some cases high Mach number). It is therefore necessary to complement such analysis and wind tunnel

tests with procedures for modeling reentry body responses from actual flight data. Such a flight test data procedure must recognize that both deterministic and stochastic effects are encountered over a series of flight tests. The procedure must extract maximum information from data, whether it is from one test or it is from several tests. These requirements are met, at least conceptually, by system identification technology.

System identification is the process of extracting mathematical model structure and parameters from a set of test data [1]. An overview of the essential steps of this process is shown in Figure 1.1. Data is first conditioned to minimize the effect of noise. Time histories of unmeasured channels are then reconstructed from available measurements. Then, an algorithm (or series of algorithms) is used to estimate the dynamic and aerodynamic factors which probably affect vehicle aerodynamics. Finally, parameter estimates are refined. (Details of this procedure are given in Chapter II.)

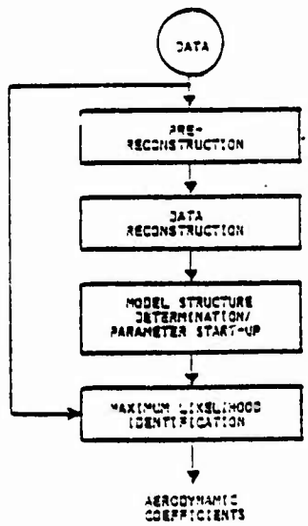

Figure 1.1 System Identification Procedure for Ballistic Reentry Vehicle Data Processing

This report summarizes the preliminary application of this system identification methodology to ballistic reentry vehicles. The ultimate objective of this application is the precise modeling of the behavior of this system to subsequently systematize its accuracy improvement.

This report is organized as follows. Chapter II reviews relevant equations of motion of a ballistic vehicle and Chapter III discusses the system identification procedure for such vehicles during reentry. Identification results for simulation data are shown in Chapter IV, and for flight test data are detailed in Chapter V. Chapter VI gives the conclusions from this effort.

1.2 PRINCIPAL DEVELOPMENTS AND RESULTS

The following major developments and results have been obtained towards the development of an integrated system identification method to estimate accurate models for aerodynamic characteristics of ballistic vehicles from limited data:

(1) An accurate reconstruction procedure is developed. This combines accelerometer and angular rate measurements to estimate the initial condition and total angle-of-attack and windward meridian time histories. The in-plane and out-of-plane moments may then be estimated.

(2) A general spline representation is developed to express the highly transient aerodynamics of the reentry vehicle. The model structure determination step is modified to select the more important terms from the general spline representation.

(3) The computer programs are modified such that mechanisms of body-fixed and wind-fixed forces and moments can be compared. In addition, a model combining the two mechanisms may also be tested.

(4) The nonlinear maximum likelihood computer program is configured to work with general ballistic vehicle aerodynamic models. This includes body-fixed and wind-fixed forces and moments.

The software was applied to a simulation data record by The Aerospace Corporation. This was followed by an application to a flight test data record.

The following preliminary conclusions are based on these applications:

(1) The algorithm application to noise-free simulated data provides basic validation of the software data processing procedure. It is found that relatively simple mathematical models can effectively represent ballistic vehicle aerodynamic phenomena for this simulated trajectory (except boundary layer transition). Since the simulated data used in this evalution was noise free, estimated parameter errors are small.

(2) The algorithm application to a single flight record demonstrated that the software could reconstruct ballistic trajectory parameters required for the development of aerodynamic models. Aerodynamic models could then be estimated. Note that the data reconstruction software compensates for bias and scale factor error in the flight data (Appendix B).

(3) The results of processing the single flight record indicate the possibility of adequately describing the boundary layer transition by a basically wind-fixed flow with a short time interval of body-fixed flow. Definitive conclusions on the general nature of vehicle forces and moments (e.g., body-fixed and wind-fixed) are not appropriate on the basis of a single flight record. Validation of this model requires analysis of further flight data.

CHAPTER II

DYNAMICS AND AERODYNAMICS OF BALLISTIC REENTRY VEHICLE FLIGHT

2.1 INTRODUCTION

The complete reentry flight of a ballistic vehicle is characterized by multiple phenomena. Above 300,000 feet, air density is low and the motion is almost purely kinematic. The aerodynamic forces become more important as the air density increases. The boundary layer is laminar at low Reynolds number flow, then goes through a transition regime to turbulent flow with increasing Reynolds number. The roll rate remains essentially constant during the high altitude kinematic motion and may speed up or slow down with the subsequent aerodynamic forces and moments.

Various designs of reentry vehicle exhibit significantly different behavior during reentry. The behavior, in general, is dependent on both the trajectory parameters (e.g. initial angle-of-attack, maximum dynamic pressure) and the reentry vehicle design (e.g. bluntness, surface roughness, etc.). In addition, significant trajectory deflections may occur in the transition region, where the boundary layer changes from fully laminar to fully turbulent. To study these trajectory deflections and related behavior anomalies and to estimate them from dynamic measurement data, a comprehensive set of vehicle dynamic equations is required.

The equations for a ballistic reentry vehicle motion have been studied by several authors previously [2-13]. This chapter reviews the dynamics of a ballistic reentry vehicle. The significant aerodynamic forces and moments are indicated, so that the resultant describing equations can serve as the basis for identifying aerodynamic effects from flight test

data. Certain useful approximations to these equations are derived specifically for use with system identification techniques of later chapters.

2.2 DYNAMICS EQUATIONS

In this section, we define reference frames commonly used in ballistic reentry vehicle (BRV) study and then review general six degree-of-freedom (DOF) equations of motion for this vehicle during atmospheric flight.

2.2.1 Reference Frames

Figure 2.1 shows three reference frames which may be used. Frame A is the wind frame, in which the X_A axis is aligned with the instantaneous velocity and Y_A is local geocentric horizontal. Frame B is the body fixed frame. The X_B axis

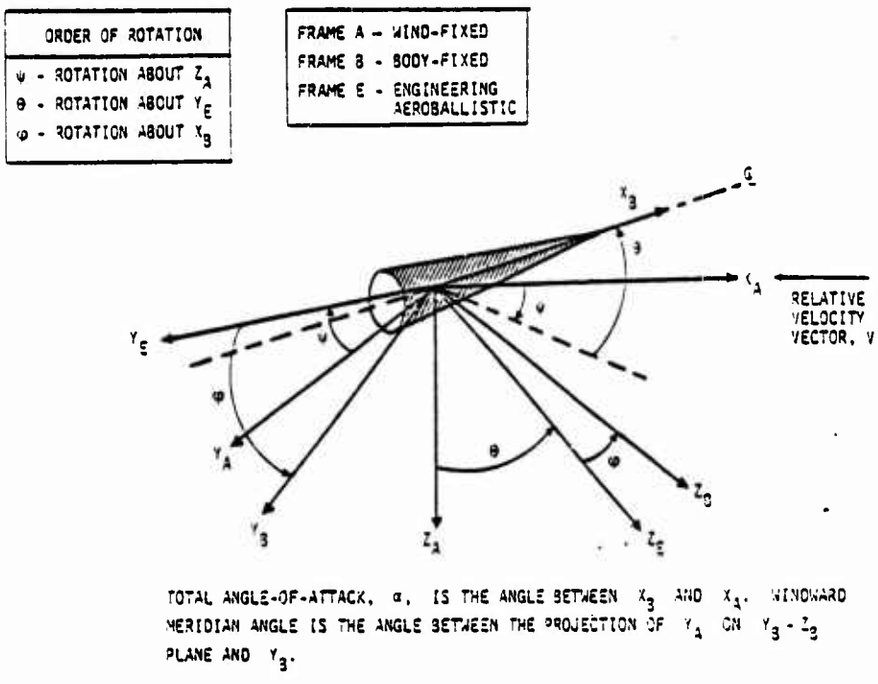

Figure 2.1 Convenient Frames for Representing Ballistic Reentry Vehicle Aerodynamics

is the axis of symmetry going through the nose and Y_B axis is aligned with a specific direction at some point in time and then fixed to the body. The engineering aeroballistic frame, E, is another body fixed frame except that it does not roll with the body. The relative orientation between the aeroballistic frame and the body frame is the body roll angle. In the engineering system, a yaw, pitch, roll sequence is used to rotate frame A through frame E to body fixed frame B. The three Euler angles are ψ, θ and ϕ. In the classical system a roll, pitch, roll sequence is used to rotate frame A into frame B giving a different aeroballistic frame. Both frames have their advantages, however, we will only use the engineering frame and engineering Euler angles. The total angle-of-attack α and the windward meridian ϕ_w are

$$\begin{aligned} \alpha &= \cos^{-1}(\cos\psi \cos\theta) \\ \phi_w &= \phi - \tan^{-1}(\tan\psi/\sin\theta) \end{aligned} \tag{2.1}$$

The wind fixed frame is not inertial. It rotates to the extent of trajectory bending. In most flights, however, the trajectory bending is negligible compared to other motions and is often neglected. Unless otherwise mentioned, in all our analysis, the wind fixed frame will be considered inertial.

2.2.2 Dynamic Equations

The six DOF equations of motion of a ballistic reentry vehicle may be written in any of the three frames discussed above. The wind frame complicates the kinematic element of the dynamic equations but the aerodynamic forces and moments are easily expressed in terms of components in the plane of the wind vector and the vehicle axis of symmetry (called in-plane) and another component orthogonal to the plane (called out-of-plane). This is useful because during a major portion of the flight, through vehicle symmetry, the forces and

moments are related to the direction of relative velocity. The on-board measurements are also difficult to express in terms of relevent dynamic variables. The aeroballistic frame is also useful under certain circumstances, for example it can easily depict the tricyclic motion of a BRV. The measurement equations and the kinematic elements of the dynamic equations are quite straightforward in the body fixed axis system. The aerodynamic in-plane and out-of-plane forces and moments must, however, be transformed through time varying angles to be used in the body fixed axis system. Chrusciel [3] uses wind fixed equations of motion. Because these equations separate out the in-plane and out-of-plane aerodynamic moments, they are easier to work with when simple estimation procedures are used. However, the body fixed equations are more useful with advanced identification procedures, because of the need to correlate multivariable measurements as accurately as possible and such accuracy is practically achieved by using untransformed measurements in the body axis system [1].

The dynamic equations of motion of a rigid reentry vehicle in the body axis system are

$$\begin{aligned}
\dot{u} &= vr - wq - g \sin\theta + \frac{q_\infty s}{m} C_x \\
\dot{v} &= wp - ur + g \sin\phi \cos\theta + \frac{q_\infty s}{m} C_y \qquad (2.2) \\
\dot{w} &= uq - vp + g \cos\phi \cos\theta + \frac{q_\infty s}{m} C_z
\end{aligned}$$

$$\begin{aligned}
\dot{p} &= \frac{q_\infty sb}{I_x} C_\ell \\
\dot{q} &= (1 - I_x/I)pr + \frac{q_\infty sb}{I} C_m \qquad (2.3) \\
\dot{r} &= -(1 - I_x/I)pq + \frac{q_\infty sb}{I} C_n
\end{aligned}$$

$$\dot{\phi} = p + q \sin \phi \tan \theta + r \cos \phi \tan \theta$$

$$\dot{\theta} = q \cos \phi - r \sin \phi \qquad (2.4)$$

$$\dot{\psi} = (q \sin \phi + r \cos \phi)/\cos \theta$$

Note that ϕ, θ and ψ are body Euler angles with respect to an inertial axis system.

These equations assume that: (1) the body is symmetric about the x axis with moment of inertia I_x, and (2) the moments of inertia about the y axis and the z axis are equal to each other. C_x, C_y and C_z are the force coefficients and C_ℓ, C_m and C_n are three moment coefficients. If the wind-fixed axes are assumed inertial, the first three equations are not required and ϕ, θ, ψ become Euler angles with respect to the wind axis system.

$$u = V \cos \theta \cos \psi$$

$$v = V \cos \psi \sin \theta \cos \phi - V \sin \psi \sin \phi \qquad (2.5)$$

$$w = V \cos \psi \sin \theta \sin \phi + V \sin \psi \cos \phi$$

where V is total speed. As mentioned previously, this is a reasonable assumption in analyzing aerodynamic moments acting on the reentry vehicle. The moment coefficients C_m and C_n may be written in terms of the in-plane (in the plane containing the wind vector and the vehicle x-axis), out-of-plane (plane perpendicular to the wind vector and containing the vehicle x-axis), and body-fixed moment coefficient. Let C_N', C_Z' and C_b be the wind-fixed in-plane and out-of-plane moments and body-fixed moment, respectively. Then,

$$C_m = C_N' \sin \phi_w + C_Z' \cos \phi_w + C_b \cos \eta$$

$$C_n = C_N' \cos \phi_w - C_Z' \sin \phi_w + C_b \sin \eta \qquad (2.6)$$

where η is the relative orientation of the body-fixed moment and the vehicle y axis. The windward meridian ϕ_w and the total angle-of-attack, as indicated earlier, are functions of the three Euler angles. In addition, θ and ψ are often small and Eqs. (2.4) can be simplified to

$$\dot{\phi} = p + \dot{\psi}$$

$$\dot{\theta} = q \cos \phi - r \sin \phi \qquad (2.7)$$

$$\dot{\psi} = q \sin \phi + r \cos \phi$$

The expressions for windward meridian and total angle-of-attack also simplify to

$$\alpha = \sqrt{\theta^2 + \psi^2}$$

$$\phi_w = \phi - \tan^{-1} (\psi/\theta) \qquad (2.8)$$

It is clear from the above discussion that accurate description of BRV dynamic motion requires models for C_ℓ, C_m and C_n. The roll equation is essentially uncoupled from the pitch/yaw equations. Roll rate behavior and roll rate anomalies may be described using a model for C_ℓ. Further approximations to the above equations may be made by assuming a constant p (i.e., $C_\ell = 0$). This reduces the number of equations to five and makes the kinematic term in the q and r equations linear. This is usually done to obtain the tricyclic motion of the reentry vehicle [6].

Models for C_m and C_n are required to describe pitch/yaw motions which are of particular interest in computing the lateral dispersions of a BRV. This report concentrates on techniques which may be used to develop such a model from flight test measurements. If, in addition, trajectory bending is required to be determined during any portion of the flight, models for C_y and C_z should also be identified. The differences between the values of v and w obtained by propagating Eqs. (2.2) and by solving Eqs. (2.5) would give trajectory bending in the body axis system. The lateral velocity components arising from trajectory bending may be directly converted into miss distance on impact.

When the boundary layer is purely laminar or purely turbulent, approximate models for C_m and C_n are known. However, much less is known in the transition region, where the boundary layer changes from completely laminar to completely turbulent over a period of time. This region is the most important from the viewpoint of the application of the state-of-the-art identification methods.

2.3 BOUNDARY LAYER TRANSITION

As the Reynolds number of a ballistic reentry vehicle increases because of increasing air density, the boundary layer at a point on the surface of the vehicle starts becoming turbulent. The transition front then proceeds to other parts of the vehicle surface. This phenomenon is called the boundary layer transition (BLT). Deterministic and random effects during boundary layer transition has been studied both theoretically and experimentally based on wind tunnel and flight tests [8-15].

Boundary layer transition front affects vehicle aerodynamic forces and moments. Transition to turbulent boundary layer is accompanied by an increased skin friction and an increased pressure in the boundary layer. If the transition were symmetric

around the body, no net moment will result on the body, though the variation of in-plane moment with angle-of-attack may change. In addition, the out-of-plane moment will be negligible. The transition is rarely symmetric, however. The asymmetry may take several forms, one example of which is shown in Figure 2.2

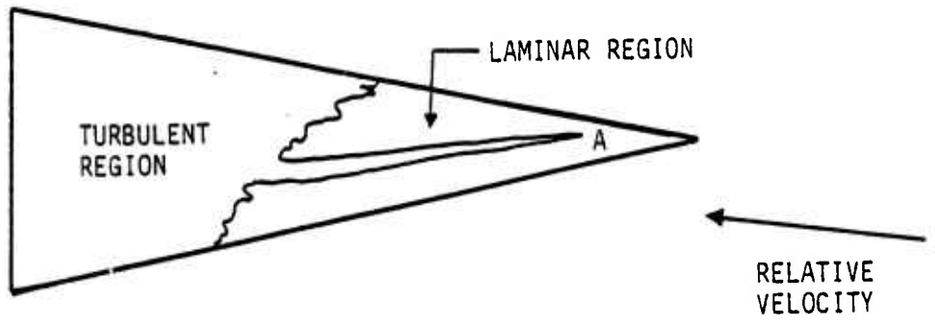

Figure 2.2 Example of Boundary Layer Transition Front

Wind tunnel tests and other studies have shown that several factors affect aerodynamic flow around a BRV during the BLT. Some of the more important variables are:

(a) cone angle of the reentry vehicle

(b) nose bluntness, ratio of nose radius to base radius

(c) nosetip and heatshield material (this determines the extent of ablation and mass addition to the boundary layer)

(d) initial roll rate, speed, and angle at reentry

(e) mass unbalance

(f) surface roughness and other surface nonuniformities (e.g. radar windows, antennas)

Moments on the vehicle during BLT cause pitch/yaw and roll rate anomalies which are not predicted by inviscid flow theory. Pitching and yawing motions of the BRV affect angle-of-attack,

producing nonzero average sideward force on the vehicle leading to trajectory bending. This trajectory bending and lateral velocity changes caused by trajectory bending are two of the most major reasons for reentry-induced impact point dispersions.

The manner in which BLT affects vehicle moments depends upon the transition pattern. Several models have been suggested for the transition phenomenon [3,14], some of which are:

(a) unstable damping coefficient

(b) asymmetric in-plane flow

(c) time-varying body fixed moment

(d) total moment lag

The consequences of these models on body moments are discussed in Table 2.1.

Table 2.1

Transition Mechanisms and Their Effects on Vehicle Aerodynamic Moments

TRANSITION MECHANISM	EFFECT ON AERODYNAMIC MOMENTS	COMMENTS
(a) UNSTABLED DAMPING COEFFICIENT	• ZERO OUT-OF-PLANE MOMENTS • SELF-EXCITED, STRONGLY DEPENDENT ON INITIAL CONDITIONS • NO EFFECT ON MOMENT VS. TOTAL ANGLE OF ATTACK CURVE	• CANNOT EXPLAIN OUT-OF-PLANE MOMENTS • CONTRADICTED BY MANY OBSERVATIONS • LOOKS REASONABLE ON A FIRST GLANCE AT THE TIME HISTORIES
(b) ASYMMETRIC IN-PLANE FLOW	• IN-PLANE MOMENT DEPENDENT ON TOTAL ANGLE-OF-ATTACK AND REYNOLDS NUMBER • ZERO OUT-OF-PLANE MOMENTS • NON-BODY FIXED	• CANNOT EXPLAIN OUT-OF-PLANE MOMENTS • MOMENTS DO NOT DEPEND UPON BODY ORIENTATION
(c) BODY IRREGULARITIES CAUSE ASYMMETRIC FLOW PATTERN	• BODY-FIXED TIME VARYING MOMENT, THE AZIMUTH OF BODY-FIXED MOMENT MAY CHANGE WITH TIME • OUT-OF-PLANE MOMENT COMPONENTS • MINOR CHANGES IN MOMENT VS. ANGLE-OF-ATTACK CURVE	• CAUSED BY SURFACE ROUGHNESS, SURFACE ASYMMETRY, ANTENNAS, JOINTS, CAUSING ACCELERATED TRANSITION TO TURBULENT BOUNDARY LAYER. DIFFERENT IRREGULARITIES MAY BE PROMINANT AT DIFFERENT TIMES.
(d) TOTAL MOMENT LAG	• TOTAL AMOUNT DEPENDENT ON AERODYNAMIC VARIABLE • PHASE LAG DEPENDENT ON WINDWARD MERIDIAN RATE • NON-ZERO OUT-OF-PLANE MOMENT	• MOMENT LAG MAY DEPEND ON WINDWARD MERIDIAN RATE AND OTHER VARIABLES

Time-varying body fixed moments are caused by small or large body irregularities. Small body irregularities, like surface roughness and joints, etc., cause random asymmetries in

BLT front. Macroscopic irregularities like antenna windows and known vehicle asymmetries produce deterministic effects on BLT. Though this moment is fixed in the body, its magnitude may change with time. In general, such a body fixed moment will lead to both in-plane and out-of-plane aerodynamic components. With reference to Figure 2.3 these components are:

$$C_N' = C_b(t) \cos[\phi_b - \phi_w(t)]$$

$$C_Z' = C_b(t) \sin[\phi_b - \phi_w(t)]$$

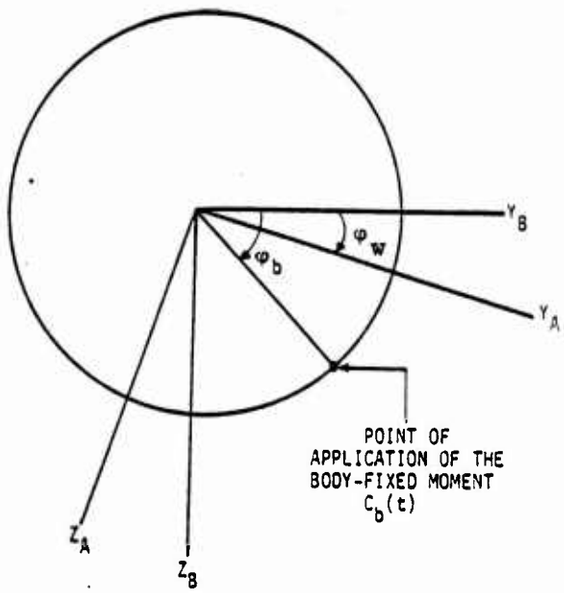

Y_A AND Z_A ARE THE PROJECTIONS OF THE WIND-FIXED AXES ON THE Y_B-Z_B PLANE.

Figure 2.3 Body-Fixed Moment Mechanism to Explain the BLT

Note that ϕ_b is a constant and $\phi_w(t)$ is a function of time. The values of $C_b(t)$ would depend upon the aerodynamic variables (e.g.

total angle-of-attack and Reynolds number) and the relative orientation of the location of the body fixed moment with wind direction. The in-plane moment will also have another component resulting from wind fixed flow.

The total moment lag mechanism is illustrated in Figure 2.4. The lag angle is a constant function of time-varying windward meridian rate and the total moment depends upon the aerodynamic variables:

$$C_N = C_m \cos\phi_L$$

$$C_Z = C_m \sin\phi_L$$

$$C_m(t) = \sqrt{C_N^2(t) + C_Z^2(t)}$$

$$\phi_L = \tan^{-1} \frac{C_Z}{C_N} = \phi_L(\dot{\phi}_w)$$

$$C_m(t) = qS\bar{c} \{C_m[\alpha(t-\tau), R_e(t-\tau)]\}$$

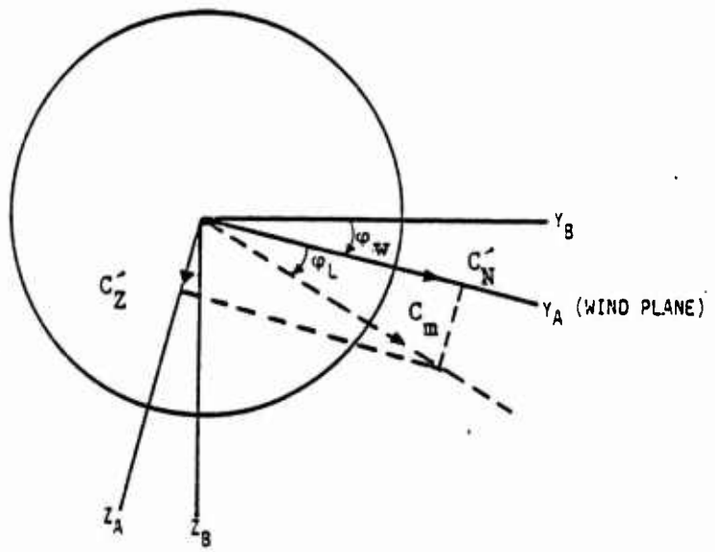

Figure 2.4 Total Moment Lag Mechanism for BLT

2.4 SUMMARY

This section describes, in brief, the dynamics and aerodynamics of flow around a BRV during reentry. Special attention is given to the BLT regime where the boundary layer changes from fully laminar to fully turbulent. The BLT regime is a combination of deterministic and stochastic effects. Though temporal and spatial random variations in flow account for some of the behavior observed during BLT, they are not useful because of their lack of predictive capability. The next section will describe state-of-the-art system identification methods which may be used to model deterministic components of "anomalous" aerodynamic moments, which are not predicted by inviscid theory. Future sections will then discuss the results of the application of the identification techniques to simulated and flight data.

CHAPTER III

SYSTEM IDENTIFICATION TECHNOLOGY FOR BALLISTIC REENTRY VEHICLES

3.1 INTRODUCTION

This section provides an overview of advanced system identification techniques for estimating aerodynamic coefficients of ballistic reentry vehicles (BRV) from dynamic flight measurements. The following major factors, characteristic to BRV, dictate requirements and limitations on applicable system identification techniques for the BLT regime:

(1) Moment and force coefficients are unknown nonlinear functions of aerodynamic variables (e.g., angle-of attack and Reynolds number).

(2) The form of dependence between the force coefficients and aerodynamic variables is not known. Several qualitative hypotheses (some of which are conflicting) have been proposed to describe the flow field under various conditions.

(3) There is no control input to the system. All state excursions (which are necessary for extraction of aerodynamic coefficients) result from non-zero initial conditions or aerodynamic model changes.

(4) Aerodynamic phenomena are possibly a combination of deterministic and random effects.

(5) Certain key variables, like total angle-of-attack and windward meridian, cannot be measured directly and must be derived from other measurements. This causes correlation between errors in derived angle of angle and other measurements.

(6) The instrument outputs are contaminated with random noise, bias and other errors.

General techniques for the development of mathematical models from test data have been discussed previously [1,16, 17]. In the following, we show how these methods are modified to be more responsive to the requirements given above. The modified procedures are applicable equally to anomalous regions like boundary layer transition and to other regions where the aerodynamics are not as complex.

Figure 3.1 gives the functional flow chart for identifying BRV aerodynamic models. A significant issue in application of

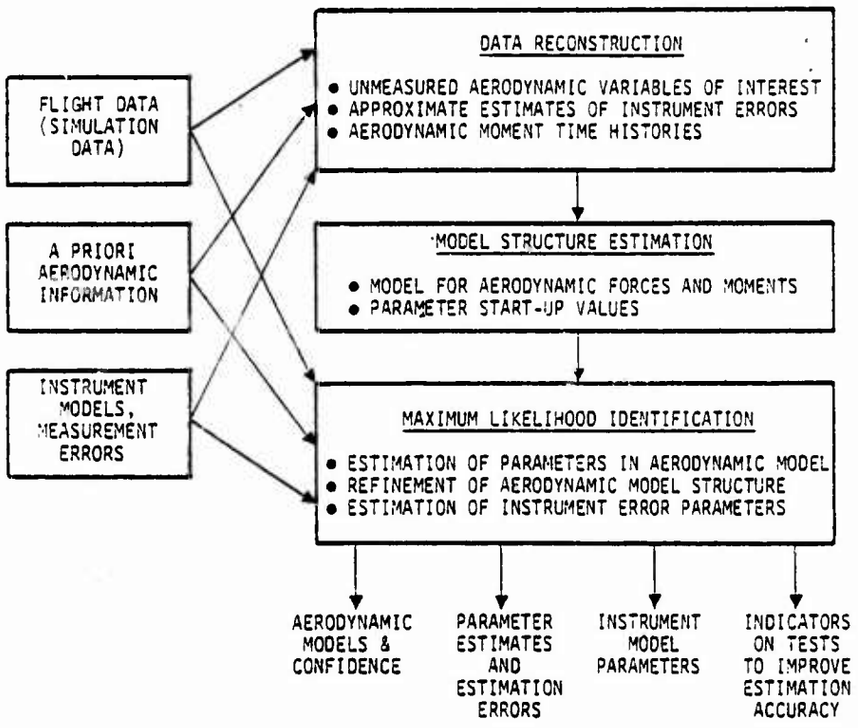

Figure 3.1 System Identification Approach for Ballistic Reentry Vehicle Aerodynamic Model Estimation

system identification to flight data is the degree to which the following steps are simultaneously performed:

(1) reconstruction of system states includes digital filtering of the data, estimation of unmeasured states, and estimation of aerodynamic force and moment time histories by open-loop integration;

(2) Model Structure Determination (MSD) by regression and hypothesis testing methods; and

(3) parameter identification of the aerodynamic models using advanced algorithms which, in addition to parameters of aerodynamic coefficient models, compute estimates of aerodynamic derivatives, their uncertainties, and sensor errors and their uncertainties.

There is a procedural ambiguity in performing these steps because each uses theoretical and computational techniques common to the other two. It is possible, for example, to perform reconstruction of system states, model structure determination, and parameter identification in one algorithm. For example, a maximum likelihood algorithm can be structured to perform all steps simultaneously. Such a structure, however, may involve significant computation burden which could be avoided by recognition of specific system characteristics such as the effect of sensor errors relative to aerodynamic uncertainties.

For the ballistic reentry vehicle system, the optimum allocation is based primarily on the relatively high quality of on-board sensors, and the resultant small errors obtainable in accelerometer and rate measurements (after the proper corrections have been applied). For small errors, the state reconstruction is optimally performed separately from the model and parameter estimation steps. Therefore, digital filtering techniques combined with efficient integration routines are suitable for this

BRV state reconstruction procedure. Model structure determination and parameter identification are best performed with a maximum likelihood identification approach.

Subsequent sections of this chapter describe briefly the above steps specifically for application to a ballistic reentry vehicle aerodynamic characteristics estimation. Details of the theory on which these steps are based may be found in Refs. 1 and 16.

3.2 DATA RECONSTRUCTION

Data reconstruction is the process of computing, from the measurements, the unmeasured quantities necessary for the identification stage. In general, it produces approximate estimates of instrument errors and a smoothed estimate of vehicle velocity components. Either concurrently or in a second stage the aerodynamic coefficients, total angle-of-attack and other variables of interest are evaluated with appropriate kinematic relationships. The objective of methods reported here is not to reassess current techniques of obtaining the best estimated trajectory (BET), nor to integrate the estimation of the aerodynamics with the trajectory reconstruction and instrument error estimation. Rather, the objective is to model the nonlinear aerodynamics as definitively as possible, such that the model based on the reconstruction will help interpret the physical phenomenon.

Typical dynamic measurements available from a BRV flight are: (a) three axis rate gyros, (b) three axis linear accelerometers, and (c) total velocity, altitude, dynamic pressure and Reynolds number from off-board measurements and BET. The reconstruction procedure is based on these measurements, but can sometimes be modified, if some of these measurements are not available.

The reconstruction problem consists of using available measurements to compute the following time histories: (a) total angle-of-attack, (b) windward meridian and rate, and (c) force and moment coefficients time histories. This problem may be subdivided into two steps: (1) estimation of initial conditions, and (2) estimation of time histories given the initial condition. These steps may be attempted sequentially or concurrently.

The reliance of the reconstruction on the BET affects the model structure determination phase but not the parameter estimation phase because the maximum likelihood algorithm is used with on-board measurements such that the instrumentation errors can be identified as well as the aerodynamic coefficient parameters.

3.2.1 Estimation of Intial Conditions

Two methods were investigated to find the initial wind plane orientation. The first method estimates the wind plane orientation prior to boundary layer transition. In the second method, the wind plane orientation and time histories of important variables are jointly estimated. One method to determine wind plane orientation and total angle-of-attack prior to BLT is given in Appendix A and another method has been described by Belknap [22].

3.2.2 Estimation of Time Histories

There are two sets of kinematic equations which are useful in time history reconstruction. Using Eqs. (2.2 and (2.4) and neglecting gravity

$$\dot{V}_b = - \underline{\omega} \times V_b + A_{cg} = -\Omega V_b + A_{cg} \tag{3.1}$$

$$\dot{\Phi} = \begin{bmatrix} 1 & \sin\phi \tan\theta & \cos\phi \tan\theta \\ 0 & \cos\phi & -\sin\phi \\ 0 & \sin\phi/\cos\theta & \cos\phi/\sin\theta \end{bmatrix} \underline{\omega} \tag{3.2}$$

where

$$V_b = \begin{pmatrix} u \\ v \\ w \end{pmatrix}, \quad \underline{\omega} = \begin{pmatrix} p \\ q \\ r \end{pmatrix}, \quad \Phi = \begin{pmatrix} \phi \\ \theta \\ \psi \end{pmatrix}, \quad A_{cg} = \begin{bmatrix} A_{cg_x} \\ A_{cg_y} \\ A_{cg_z} \end{bmatrix}$$

In the reconstruction procedure, noisy values of ω and A_{cg} are substituted in Eqs. (3.1) and (3.2). One of three methods described below may be used to obtain the total angle-of-attack and the windward meridian time histories using these equations.

Method 1

The body fixed system is aligned with the body at the initial point such that the x-axis lies along the axis of symmetry and the y-axis points along the input direction of y accelerometer. The three velocity components are determined at the initial point from the algorithm of Section 3.2.1.

Equation (3.1) is then propagated to obtain the time histories of u, v and w. Alternatively, only the v and w equations may be propagated and the total velocity used from off-board measurements. The total angle-of-attack and windward meridian are computed from v and w as follows

$$\alpha = \arctan \frac{\sqrt{v^2 + w^2}}{u} \tag{3.3}$$

$$\phi_w = \arctan (w,v) \tag{3.4}$$

Windward meridian rate is obtained by differentiating Equation (3.4) and substituting from Equation (3.1) where necessary.

If the inertial axis is fixed to the initial direction of the velocity vector, then propagation of Equation (3.2) gives the orientation of the BRV in the inertial axis system.

A major problem with this technique is that Equation (3.1) are neutrally stable, therefore measurement errors tend to build up in integration. (Note that the transition matrix Ω is singular.) The other two methods attempt to avoid this problem by assuming that the trajectory bending is insignificant.

Method 2

The trajectory bending during any short portion of the flight is assumed insignificant and may be neglected for the purpose of estimating the aerodynamic moment coefficients. Eq. (3.2) may then be used with Eqs. (2.5) and Eqs. (3.3) and (3.4) for estimation of total angle-of-attack and windward meridian.

This is the angular rate method of Belknap [22]. If a small angle assumption is also made, Eqs. (3.2) are used with Eq. (2.8) repeated here for convenience:

$$\alpha = \sqrt{\theta^2 + \psi^2}$$

$$\phi_w = \arctan(\psi, \theta) \tag{3.5}$$

Method 3

This method also assumes no trajectory bending and uses both Equations (3.1) and (3.2). Equation (2.5) are applied to set up a filtering formulation in which results of (3.1) and (3.2) are cross checked with each other and corrected if necessary at each measurement point. This is the most accurate technique and can effectively filter out measurement errors in the accelerometers and rate gyros.

3.2.3 Joint Estimation of Initial Conditions and Time Histories

Advanced filtering techniques enable simultaneous estimation of initial conditions and time histories of important aerodynamic variables. This is accomplished by using Method 3 above and considering initial conditions as unknowns in the filter. Because the equations are nonlinear and coupled, several filter passes through the data are necessary.

3.2.4 Estimation of Force and Moment Coefficients Time Histories

Force coefficients are evaluated in the body frame using body accelerations at the center-of-gravity. They are then rotated to an in-plane and out-of-plane component with the

windward meridian. The body frame moment coefficients are computed by:

$$\begin{bmatrix} C_{\ell} \\ C_m \\ C_n \end{bmatrix} = [I\dot{\underline{\omega}} + \underline{\omega} \times I\underline{\omega}] \begin{bmatrix} 1/b & 0 & 0 \\ 0 & 1/b & 0 \\ 0 & 0 & 1/b \end{bmatrix} \frac{1}{q_{\infty} S}$$

The moment coefficients C_m and C_n are also rotated using the windward meridian angle, to an in-plane moment C_N' and out-of-plane moment C_Z'.

3.3 MODEL STRUCTURE DEVELOPMENT

The model structure development is an extremely important stage in the overall system identification approach for BRV flight data processing. A good model, at minimum, (1) gives insight into the applicable physical phenomenon, (2) explains the anomalous moment (moments which cannot be explained by inviscid flow), and (3) is capable of predicting the nonlinear aerodynamics in the neighborhood of the flight trajectory. The model obtained from a single flight test can only describe those parts of the flight regime through which the vehicle travelled. Therefore, a model for BRV flight phenomena will not be complete without extensive, interactive evaluation of many flights. However, as the results reported in the following chapters indicate, it is possible to develop, based on one flight, models which interpret the moment behavior. These results can also offer inputs for the design and deployment of future experimental flights.

The model structure determination problem is to explain the behavior of aerodynamic coefficients time histories in terms of independent aerodynamic variables of interest, functions of these variables, or variables which could explain a particular physical phenomenon (e.g. a nonsymmetric flow sticking to the BRV surface during BLT).

In general, model structure determination may be divided into three distinct subproblems (see Ref. 29 for details):

(1) Selections of general functional forms to relate the moments and forces to independent variables for use with noisy test data.

(2) Criteria to compare competing models in order to determine the model with the best predictive and other capabilities for a class of responses.

(3) Efficient computational techniques for determining the models from test data.

3.3.1 Selection of General Functions

The first subproblem deals with determining the least complex, but most effective, model for predicting system response. The linear model, for example, is often the least complex of models (if the number of required linear terms is not excessive), but will be limited in predicting nonlinear response characteristics. The nonlinear model, alternately, may be more complex, but has better predictive capability. The most general formulation, therefore, involves selection of general nonlinear functions which can approximate a wide class of unknown linear or nonlinear relationships. Taylor series polynomials, orthogonal polynomials, and Chebyshev polynomials have been used previously with good success in limited examples. Recent results, presented in this report, show that a new formulation, based on splines with optimal knots, provides nonlinear models of high generality.

The advantage of spline functions is that a certain set of discontinuities can be included allowing the model to represent, and hence interpret, rapid changes in the underlying physical phenomenon. A representation for the spline function $S_{m,\nu}(x)$ used to represent the true aerodynamic coefficient $C_{aero}(x)$ is due to Greville [23]

$$C_{aero}(x) \approx S_{m,\nu}(x) = \sum_{j=0}^{m} C_{1j} x^j + \sum_{\ell=2}^{k} \sum_{j=\nu+1}^{m} C_{\ell j} (x-x_\ell)_+^j \tag{3.6}$$

where x_+^j is the truncated power function

$$x_+^j = \begin{cases} x^j & x \geq 0 \\ 0 & x < 0 \end{cases} \tag{3.7}$$

where m is the polynomial order and ν the order of continuity.

The specification of the approximating splines requires the selection of four variables: (a) m and ν, (b) number and position of knots, (c) specific terms which could be deleted, and (d) coefficients C_{ij}. The spline representation is linear in unknown parameters C_{ij}. This facilitates applications of the techniques discussed in the following subsections (see also Ref. 24).

3.3.2 Model Selection Criteria

Development of useful criterion to compare competing models is probably the most difficult of the three problems. Several criterion for application to BRV aerodynamic model development were reviewed and extended in this work. These include:

(a) residual sum of squares,
(b) adjusted residual sum of squares,
(c) prediction error,
(d) Mallow's C_p,
(e) total equation F-ratio,
(f) average expected variance, and
(g) Allen's prediction error at a point.

All these criteria have advantages and disadvantages. For detailed discussions see Ref. 25. Total F-ratio was used as the primary criterion in this application and the prediction error was used as a cross check. The importance of engineering judgement and its application in choosing good subsets as models is discussed and illustrated with simulation data in Section IV and with flight data in Section V.

3.3.3 Computation Techniques

Efficient computational techniques are an integral part of a successful MSD procedure. Often there are many data points and many possible independent variables or functions of independent variables which may explain the dependent variable. To implement the MSD procedure, therefore, the computation method must require reasonable computation time and storage. In engineering practice, a suboptimal model is often acceptable, if the computational time required to obtain a slightly better model is too high. Two methods have been successfully applied, both based on the regression technique. The first method takes less computational time and storage, but does not necessarily give the optimal model. Stepwise, subset regression [26] is an iterative procedure which starts by including the most highly correlated variable in the regression. At every step, hypothesis testing is done to determine if any new variable should be included in the regression or if any of the variables already in the equation should be dropped. The

partial F-value, defined as the ratio of improvement in fit produced by entering a variable in the regression to the total fit error, corrected for the degrees of freedom, is computed for each parameter. The cut-off F-value is determined from the F-distribution based on a certain confidence level. A comparison of the partial F-value with the cut-off value gives the parameters which may be included in the equation or dropped from the equation. The values of the coefficients are computed simultaneously.

The optimal regression technique, called "regression by leaps and bounds" [27] finds the best regressions without examining all possible combinations and gives the best subsets for each number of parameters included in the model. The subsets are evaluated based on the criteria given in Section 3.3.2 to determine the optimal size.

3.4 MAXIMUM LIKELIHOOD TECHNIQUE FOR PARAMETER IDENTIFICATION

The model structure development phase gives good models for aerodynamic coefficients but the values of the parameters are not accurate. In addition, the MSD phase uses reconstructed data which may be contaminated with instrumentation errors and BET estimation errors. The maximum likelihood parameter identification step estimates the parameters of the model from the previous step. Significant instrument errors are estimated simultaneously to minimize their effect on parameter estimation errors.

The maximum likelihood method is very general and comprehensive. Conceptually, it can be summarized as follows:

> "Find the probability density functions of the observations for all possible combinations of unknown parameter values. Select the density function whose value is highest among all density functions at the measured values of the observations. The corresponding parameter values are the maximum likelihood estimates."

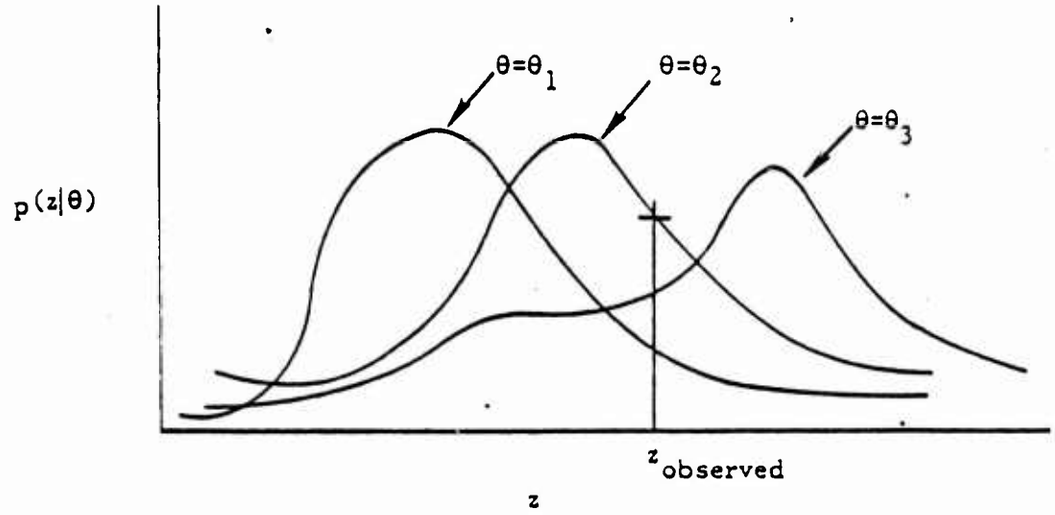

Figure 3.3 Maximum Likelihood Estimates

Suppose θ can take three possible values: θ_1, θ_2, and θ_3. Let the probability density functions of observations z for these three values of θ be as shown in Figure 3.3. Then, if the actual observation is z, θ_2 is the maximum likelihood estimate of θ. In practice, starting from a priori estimates, the parameters are updated so that the value of the resulting density function at the observations increases monotonically

Suppose we make a series of observations y(1), y(2)..y(N), called Y(N), which are functions of an unknown parameter vector θ. Then the likelihood function for parameter θ is the conditional probability density function of Y(N) given θ. The negative log-likelihood function (NLLF), -log p(Y(N)/θ), may be written as

$$\begin{aligned} \text{NLLF} &= -\log p(Y(N)|\theta) \\ &= -\log \prod_{i=1}^{N} p[y(i)|Y(i-1),\theta] \qquad (3.9) \\ &= -\sum_{i=1}^{N} \log p[y(i)|Y(i-1),\theta] \end{aligned}$$

This formulation is particularly useful for dynamic systems where the observations y(1), y(2)..y(n) can be ordered with increasing time. The conditional probabilities lead directly to a two-stage formulation, the first stage of which is a Kalman filter, dependent on unknown parameter values, and the second stage is a function of the Kalman filter output. It is straight-forward to show that [16], for white gaussian process and measurement noise sources

$$NLLF = \sum_{i=1}^{N} \{\nu^T(i)B^{-1}(i)\nu(i) + \log|B(i)|\} \qquad (3.10)$$

where $\nu(i)$ are the innovations at measurement point y(i) and B(i) is the covariance of $\nu(i)$. Both $\nu(i)$ and B(i) are outputs of the Kalman filter and are, in general, functions of unknown parameters. The procedure, based on maximizing the likelihood function or minimizing the NLLF, therefore, involves minimizing a function of the output of a Kalman filter, which depends upon unknown parameter values. If the gradient based techniques are used, we must compute the first and possibly the second gradient of NLLF. Exact expressions for this are complex but several approximations enable an engineering solution. First B(i) is assumed time invariant and is estimated by differentiating NLLF with respect to B.

$$\hat{B} = \frac{1}{N} \sum_{i=1}^{N} \nu(i)\nu^T(i) \qquad (3.11)$$

This reduces NLLF to,

$$NLLF = \frac{1}{2} \sum_{i=1}^{N} \nu^T(i)\, \hat{B}^{-1}\nu(i) \qquad (3.12)$$

The first and second gradients of the simplified NLLF are, approximately,

$$\frac{\partial(\text{NLLF})}{\partial\theta} = \sum_{i=1}^{N} \nu^T(i)\, \hat{B}^{-1}\, \frac{\partial\nu(i)}{\partial\theta} \tag{3.13}$$

$$\frac{\partial^2(\text{NLLF})}{\partial\theta^2} \approx \sum_{i=1}^{N} \frac{\partial\nu^T(i)}{\partial\theta}\, \hat{B}^{-1}\, \frac{\partial\nu(i)}{\partial\theta} \tag{3.14}$$

Thus we need the gradients of the innovations as time functions which requires the propagation of the Kalman filter and its sensitivities. The gradient method iterations are continued until NLLF cannot be decreased by changing the parameters. Ref. 30 discusses the computational problem in detail.

For the BRF problem, the actual process noise (gusts, random atmosphere density changes, etc.) is quite low such that ML estimation with an output error formulation should work well. The software adapted for the BRV problem is versatile. Aerodynamic coefficients C_x, C_{y_C}, C_{z_C}, C_ℓ, C_Z', C_N', are linear or nonlinear functions represented by a polynomial expansion of the form

$$C_k = \sum_{j=\ell_1}^{\ell_2} P_j \prod_{i=1}^{m} (z_i - z_{i_o})^{n_{ij}}$$

where

P_j is a parameter which may be identified by the program

z_i is an expansion variable (a function of states), which varies from region to region

z_{i_o} is the reference value of the ith expansion variable, and

n_{ij} are integer exponents of the expansion variables.

This type of representation of completely different nonlinear models specified completely by input has been adapted to include spline function models. The purpose is still the same, to refine the spline coefficients, and the program can also modify the model structure somewhat by identifying certain knot locations more accurately.

The coefficient time histories and their variances are computed from the optimal parameter value of $\underline{\theta}^*$

$$C_m = \underline{f}^T(\underline{x})\underline{\theta}^*$$

$$\text{Cov}(C_m) = \underline{f}^T(\underline{x})M^{-1}\underline{f}(\underline{x})$$

$$\underline{f}(\underline{x}) = [f_1(\underline{x}),\ f_2(\underline{x}),\ldots,f\ (\underline{x})]^T$$

where $\underline{f}(\underline{x})$ is a vector of the functions included in this model. Similarly, the dimensional stability derivatives and their covariances are evaluated by

$$M_{x_i} = \frac{\partial C_m}{\partial x_i} q_s C' = q_s C\ (\partial \underline{f}/\partial x_i)^T\ \underline{\theta}^*$$

M_{x_i} is the dimensional stability derivative of C_m with respect to x_i (x_i is a state variable or a function of state variables).

3.5 SUMMARY

In the identification of nonlinear systems, the model structure determination phase is extremely important and requires the reconstruction of related but unmeasured aerodynamic variables and coefficients. This phase develops the model and gives initial estimates of parameters in this model. The maximum likelihood parameter estimation stage uses these

model structures but goes back to the original measurements to obtain asymptotically unbiased and minimum variance estimates of the parameters (under the assumption that the model structure is exact).

CHAPTER IV

AERODYNAMIC MODEL IDENTIFICATION FROM SIMULATED DATA

4.1 INTRODUCTION

Application of the software based on the advanced system identification procedure of the previous section to simulation data is necessary not only to demonstrate capabilities of the techniques but also to verify the software. The simulation data used in this study is obtained from General Trajectory Simulation (GTS), an advanced computer program developed by Aerospace [28]. GTS uses complex aerodynamic force and moment coefficient models and can simulate aerodynamic flights of ballistic vehicles under a variety of conditions. Three time histories of BRV simulated measurements were supplied by Aerospace to SCI (Vt). The simulated data is generated for a ballistic vehicle trajectory at 200 samples per second. The measurements are noise free. The data tape also contains aerodynamic variables not available in flight. These variables are used to verify the software but are not used in the identification as such.

The following sections describe the results of processing a data record. Time histories of a typical angular rate and a typical linear accelerometer measurement are shown in Figure 4.1. Since the measurements are noise free, the data is only used to verify the software, but it is not used to evaluate coefficient estimation errors.

4.2 DATA RECONSTRUCTION

The rate integration method is used to compute the pitch and yaw angles. Figure 4.2 shows a cross plot of reconstructed

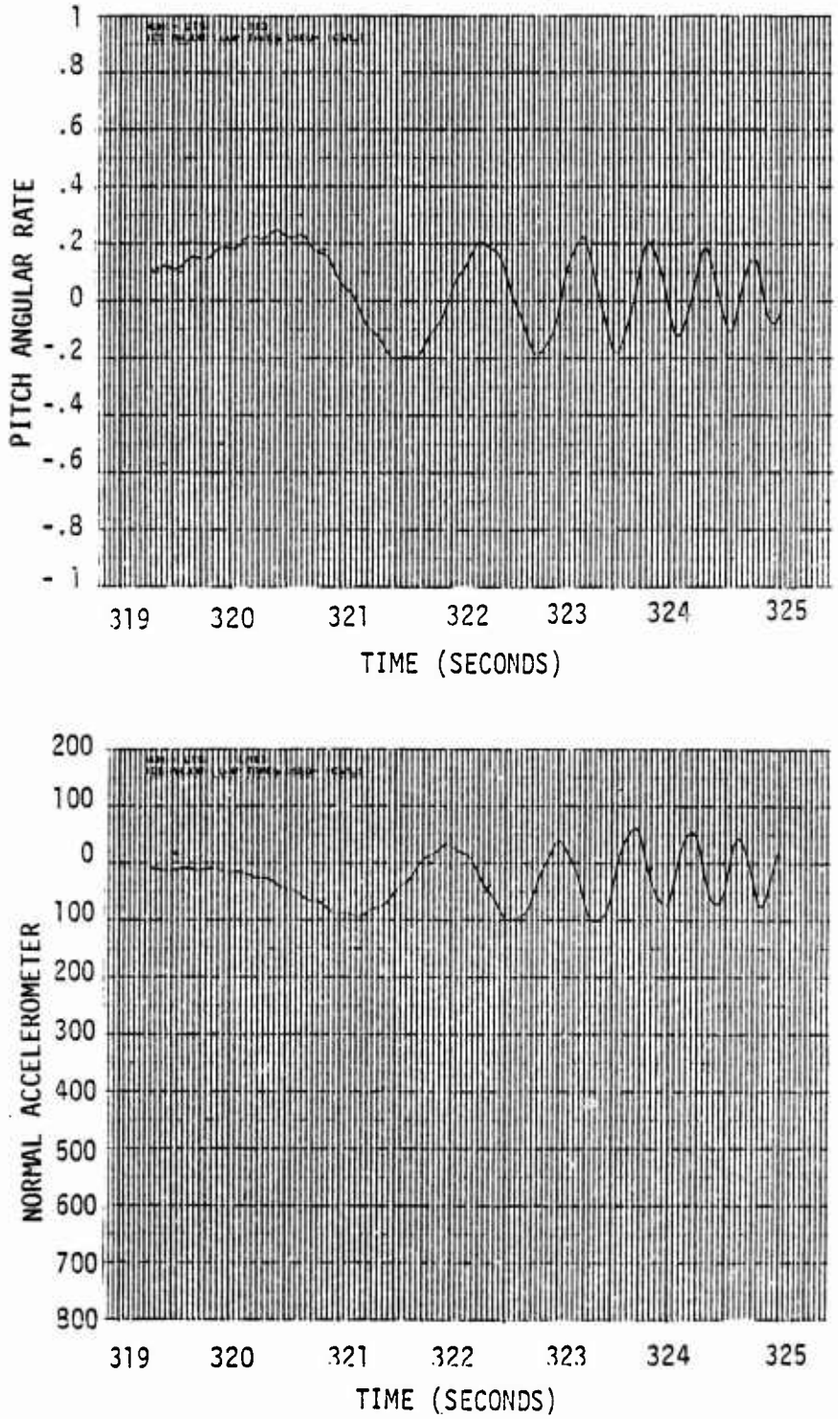

Figure 4.1 Typical Accelerometer and Angular Rate Time Histories

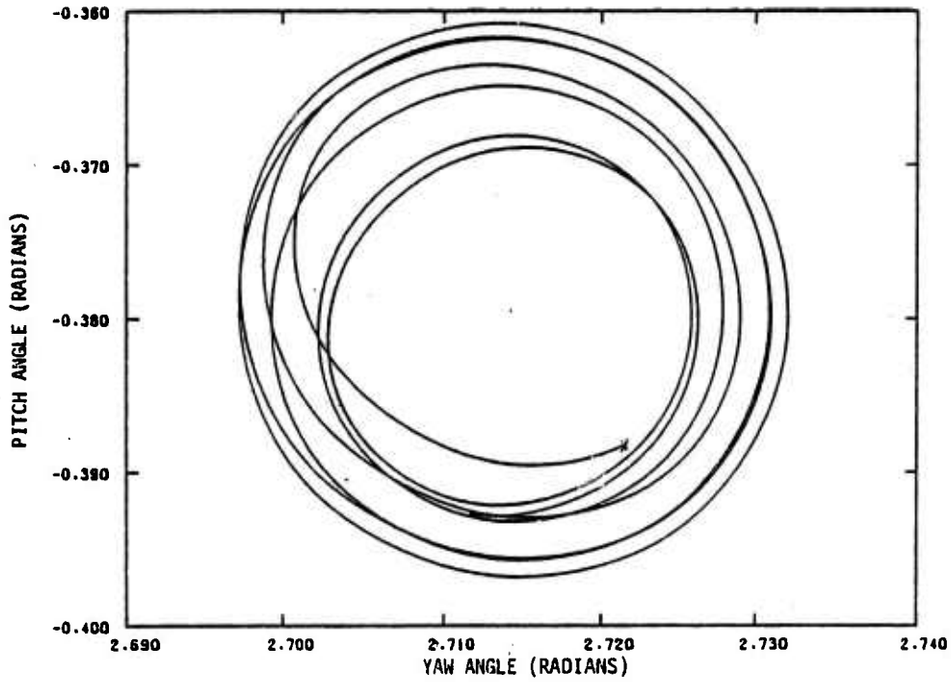

Figure 4.2 Reconstructed θ/ψ Cross Plots
TALO 319.33 to TALO 322.32

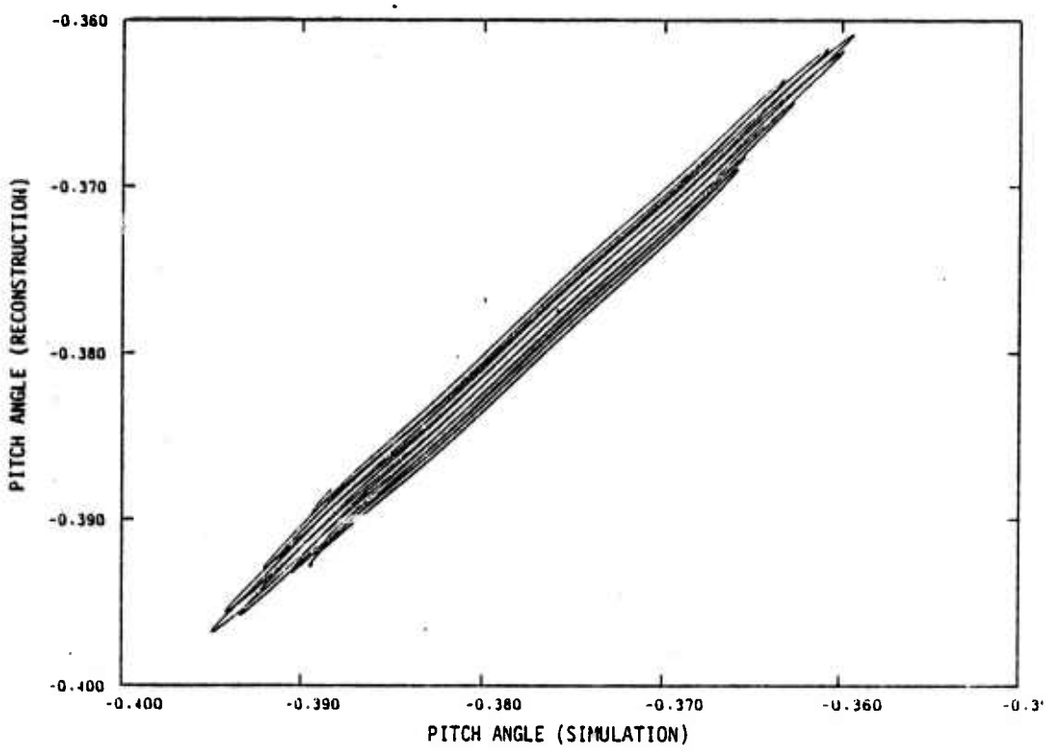

Figure 4.3 Reconstructed Vs. Simulation Pitch Angle
TALO 319.33 to TALO 322.32

pitch and yaw angles. The vehicle nose is moving in near perfect circles. Averaging pitch and yaw angles over two cycles determines the initial wind plane orientation in the body axis system and the initial total angle-of-attack. Note that the assumption of no trajectory bending is implicitly made in the rate integration method. The reconstructed pitch and yaw angles are compared to the simulation values in Figures 4.3 and 4.4. The fits are quite good considering that pitch and yaw angles are obtained through straight integration. Figure 4.5 compares the reconstructed pitching moment coefficient and the corresponding simulation values. The reconstructed out-of-plane moment is very small and was neglected. The time histories of the following variables were generated in the reconstruction stage:

(1) pitch and yaw angle,
(2) total angle-of-attack,
(3) windward meridian,
(4) windward meridian rate,
(5) in-plane and out-of-plane moment coefficients, and
(6) in-plane and out-of-plane force coefficients.

Reconstruction was also performed by propagating the three linear velocity equations in the body axis system [Eqs. (2.2)]. A steady divergence in the estimated velocity component was noted. This observation agrees with the analysis of Chapter III. It was concluded, therefore, that the rate integration method is the preferred technique. This calculation also verified the data reconstruction software.

4.3 MODEL STRUCTURE DEVELOPMENT

The aerodynamic model on which the GTS generated simulation data is based is complex and is not useful for identification; it is not identifiable from the dynamic measurements taken on a

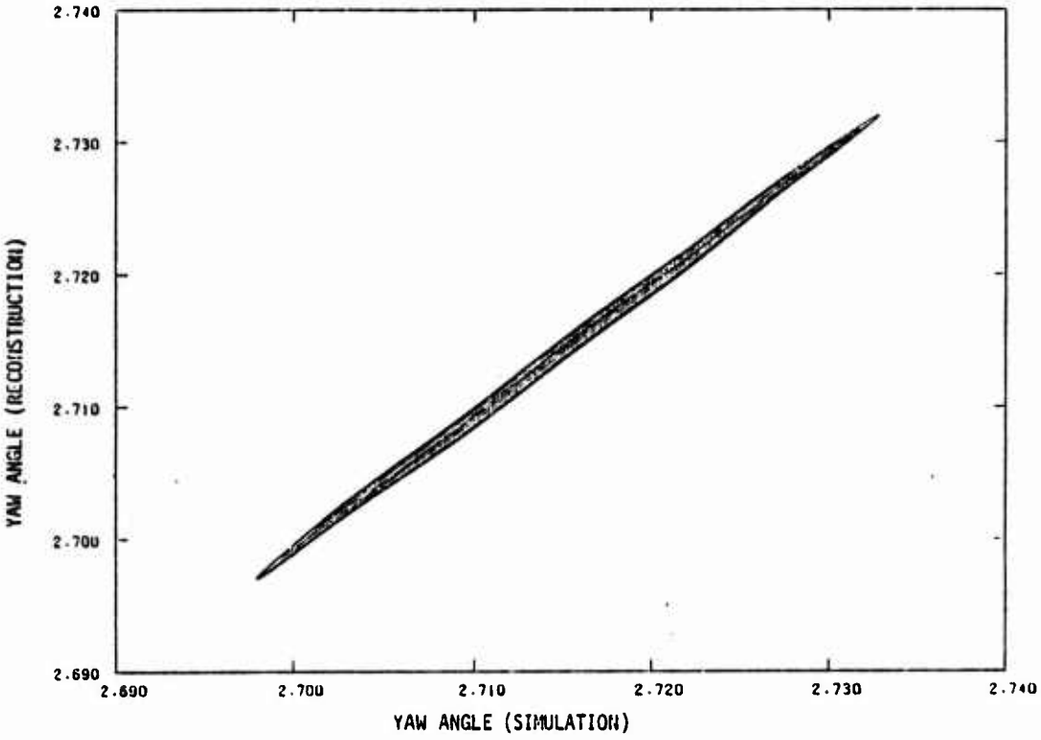

Figure 4.4 Reconstructed Vs. Simulation Yaw Angle
TALO 319.33 to TALO 322.32

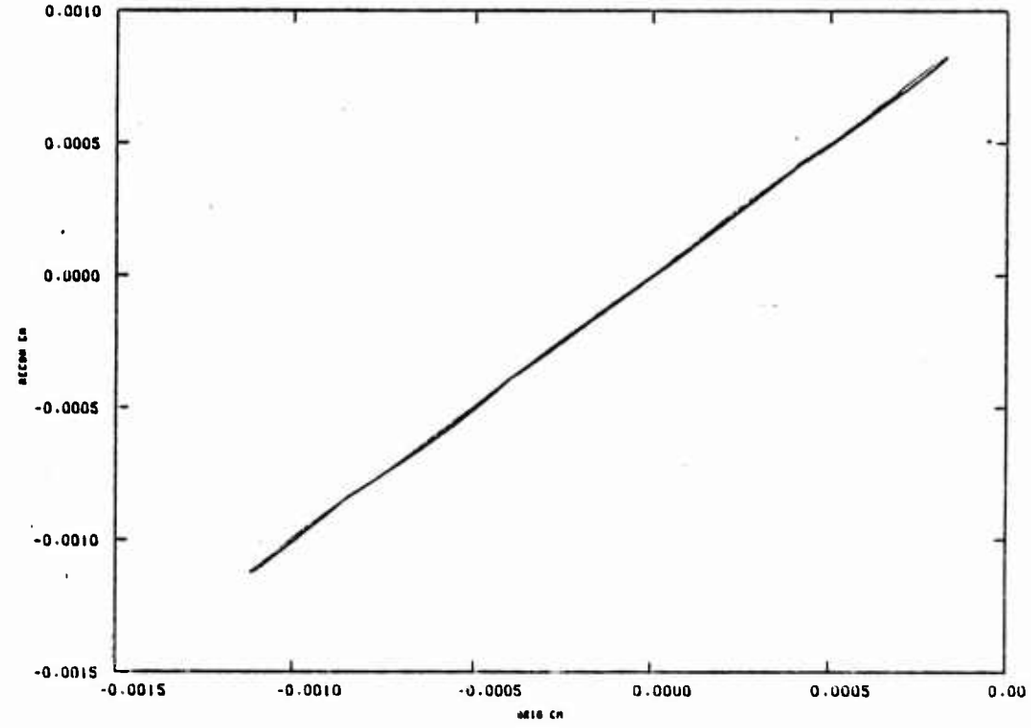

Figure 4.5 Reconstructed Vs. Simulation Pitching Moment Coefficient
TALO 319.33 to 322.32

single flight. The main reason for nonidentifiability is that the GTS model holds over the entire range of flight conditions while the dynamic model is just one realization through the flight envelope. Also, the form of the simulation model is not known to SCI (Vt). It is known, however, that the aerodynamic coefficients are functions of the angle-of-attack, Reynolds number and Mach number.

As pointed out in the previous chapter, the optimal subset regression method requires the specification of a maximal model. The maximal model selected here is a general polynomial in total angle-of-attack (α), Reynolds number (Re), and Mach number (μ), shown in the first column of Table 4.1.

The models isolated by the regression technique for the in-plane moment and force coefficients during TALO 319.33 sec to TALO 322.32 sec are indicated in the second and third columns of Table 4.1, respectively. A blank entry indicates that the corresponding term is not included in the model. The table shows that a model with seven terms can explain about 99.99% variation in the in-plane moment coefficient and two terms can explain almost all the variation in the in-plane force coefficient. It indicates that even though the normal force coefficient depends primarily on angle-of-attack, the center of pressure is a more complex function of angle-of-attack, Reynolds number and may have a weak dependence on Mach number.

Table 4.2 shows the order in which the variables enter the in-plane moment coefficient equation. Total angle-of-attack is the most important variable and enters the equation first. Reynolds number is the next in importance and it, together with total angle-of-attack, explains about 99% variation in the in-plane moment coefficient. The next two terms increase the explained variation to better than 99.95%. The overall equation F-value is high showing good confidence in the

Table 4.1

Nonlinear Terms Considered to Model the In-Plane Force and Moment

NONLINEAR TERM*	$C_{\tilde{N}}$	C_{Z_C}
Constant	-0.00101	-0.0128
α	-0.0695	-0.859
Re	0.000226	
μ		
α^2		
α^3		
α^4		
Re^2	-0.0000108	
Re^3		
$\alpha\mu^3$		
αRe	0.0125	
μ^2		
μ^3		
$\alpha\mu$		
$Re\mu$		
$\alpha^2 Re$		
$\alpha^2\mu$		
$\alpha\mu^2$		
$Re\mu^2$		
αRe^2	-0.00685	
μRe^2		
$\alpha^3 Re$		
$\alpha^3\mu$		
$\alpha^4 Re$		
$\alpha^2 Re^2$		
$\alpha^2\mu^2$		
$Re^2\mu^2$	-0.0976	
$\alpha Re\mu$		
VARIATION EXPLAINED:	99.99%	100.00%

*$\alpha = \alpha_T - \bar{\alpha}$; $\bar{\alpha} = 0.0143$

$Re = Re_T - \overline{Re}$; $\overline{Re} = 1.939$ (Normalized with $Re_o = 3.71$ Million)

$\mu = \mu_T - \bar{\mu}$; $\bar{\mu} = 0.983$ (Normalized with $V_o = 23{,}200$ fps)

estimated equation. The overall F-value for the in-plane force coefficient is also high. These exceptionally high equation F-values are obtained because of noise-free data.

Table 4.2

Steps in the Development of Model Structure for In-Plane Moment Coefficient

STEP NUMBER	VARIABLE* ENTERED	VARIATION EXPLAINED		TOTAL F-VALUE
		R	R^2	
1	α	0.885	0.783	0.216 + 03
2	Re	0.995	0.990	0.287 + 05
3	Re^2	0.9997	0.9990	0.314 + 06
4	αRe	0.9998	0.9997	0.433 + 06
5	$Re^2\mu^2$	0.9999	0.9998	0.618 + 06
6	αRe^2	0.9979	0.9999	0.164 + 07

*$\bar{\alpha}$ = 0.0143

$\bar{Re}$ = 1.939 (Re_o = 3.71 Million)

$\bar{\mu}$ = 0.963 (V_o = 23,200 fps)

4.4 MAXIMUM LIKELIHOOD PARAMETER ESTIMATION

The model developed in the previous section of the in-plane force and moment coefficients is further refined using the maximum likelihood technique. Note that the out-of-plane moment and force were so small that they are assumed to be zero. The measurements used in likelihood estimation are from the three-axis rate gyros and linear accelerometers.

Reconstructed variables are not used in the maximum likelihood parameter estimation stage since these variables are derived from rate gyro and linear accelerometer measurements. Pitch rate, yaw rate and three Euler angle equations are integrated, while roll rate is taken directly from the measurement. In addition, normal and side velocities equations are also integrated. The sensor equations currently available in the Non-Linear Systems Control Maximum Likelihood Identification (NLSCIDNT) program for use on ballistic aerodynamics are given in Appendix B. Any subset of these sensors may be chosen in any application.

Maximum likelihood parameter estimates are compared with regression estimates in Table 4.3. There are some differences. The reason is as follows. The regression program used for

Table 4.3

In-Plane Moment (C_N) and Force (C_{Z_C}) Coefficients

COEFFICIENT	REGRESSION	MAXIMUM LIKELIHOOD		
	VALUE	VALUE	STD. DEV.	F-RATIO
C_{N_o}	-0.00101	-0.00103	0.00000204	252258
C_{N_α}	-0.0695	-0.0615	0.000626	9647
$C_{N_{Re}}$	0.000226	0.000243	0.000000741	107569
$C_{N_{Re^2}}$	-0.0000108	0.0000285	0.00000662	19
$C_{N_{\alpha Re}}$	0.0125	0.0237	0.000665	1304
$C_{N_{\alpha Re^2}}$ ...	-0.00685	-0.00981	0.00177	31
$C_{N_{Re^2\mu^2}}$ ...	-0.0976	-0.143	0.0140	105
$C_{z_{C_o}}$	-0.0128	-0.0115	0.0000381	91008
$C_{z_{C_\alpha}}$	-0.8594	-0.976	0.0144	4586

model development is efficient computationally and it is a suboptimal stepwise algorithm. This is confirmed by comparing the maximum likelihood F-values in Table 4.3 with the order the terms entered the model in Table 4.2. The terms of highest F-value (in order of decreasing F-value) are constant Re, α, and αRe, yet the stepwise program did not select the model in this order. These are the types of terms that would be expected to represent the aerodynamics in this region.

Figure 4.7 shows the gyro and accelerometer measurements and estimates based on the maximum likelihood model of Table 4.3. Figure 4.8 indicates variation in normalized velocity and normalized Reynolds number (nromalized to the first point on the trajectory, where velocity is 23,200 fps and Reynolds number is 3.71 million).

Figure 4.9 shows the true value of the in-plane moment and Figures 4.10 through 4.12 show the estimated in-plane moment and its stability derivatives with respect to the total angle-of-attack and Reynolds number. Also shown are two standard deviations of estimation errors. The uncertainty in the stability derivatives represents the uncertainty in estimating away from the simulation trajectory. This uncertainty quantifies the predictive character of the model. Both stability derivatives of Figures 4.11 and 4.12 show an increase in uncertainty in approximately the last 0.5 sec. This is clearly the result of including the higher order terms with Reynolds number (see Table 4.2), Re^2, $Re^2\mu^2$, and Re^2. In this latter portion of the trajectory (t = 321.82 - 322.32), Reynolds number squared nearly doubles, making the Re^2 terms much more significant. Thus, in Figure 4.10, the total in-plane moment, the uncertainty is greater during the latter portion. If the data were extended beyond 322.32, the uncertainties during the latter portion of time would decrease.

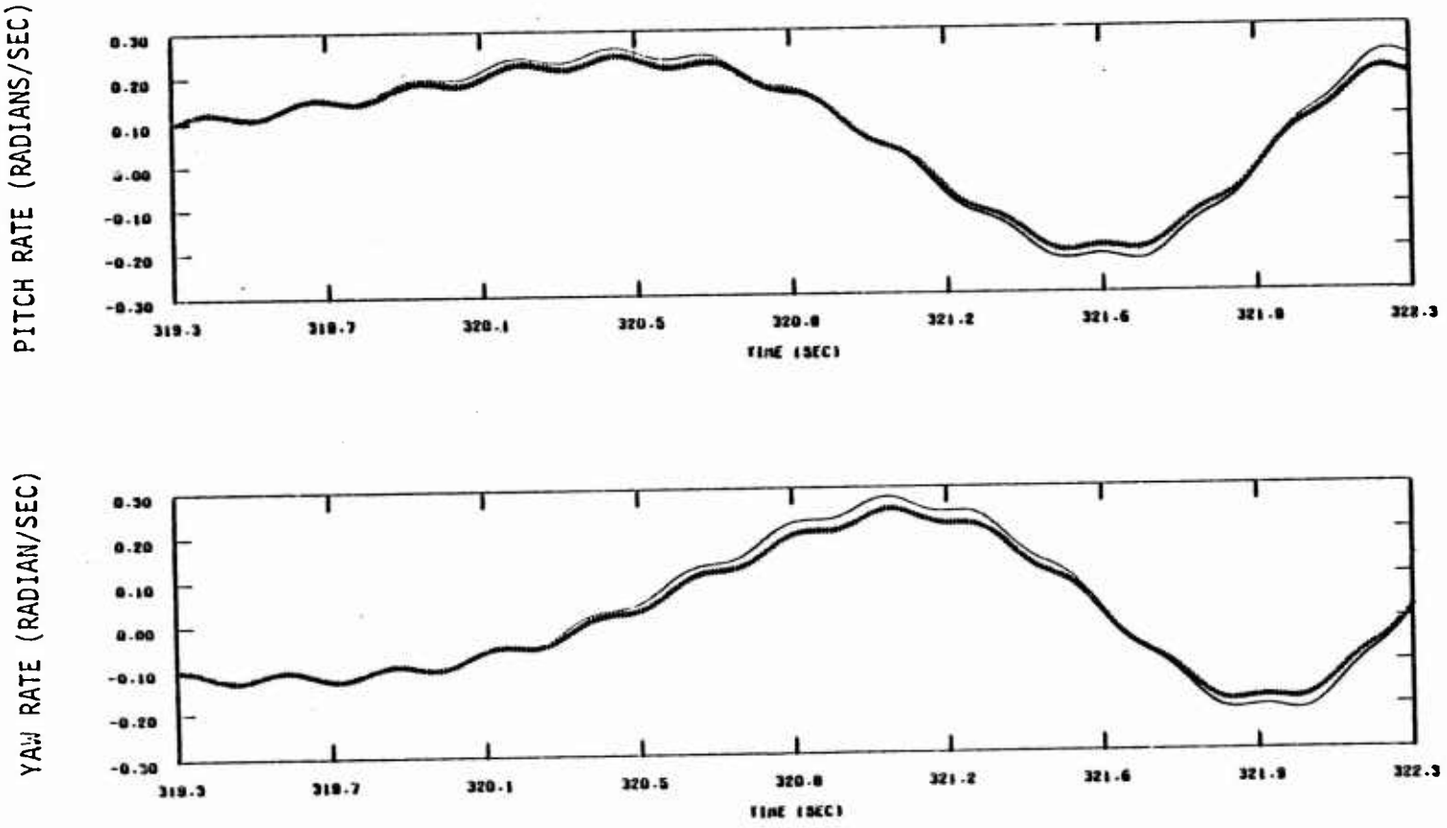

Figure 4.7 Measured and Estimated Pitch and Yaw Rates

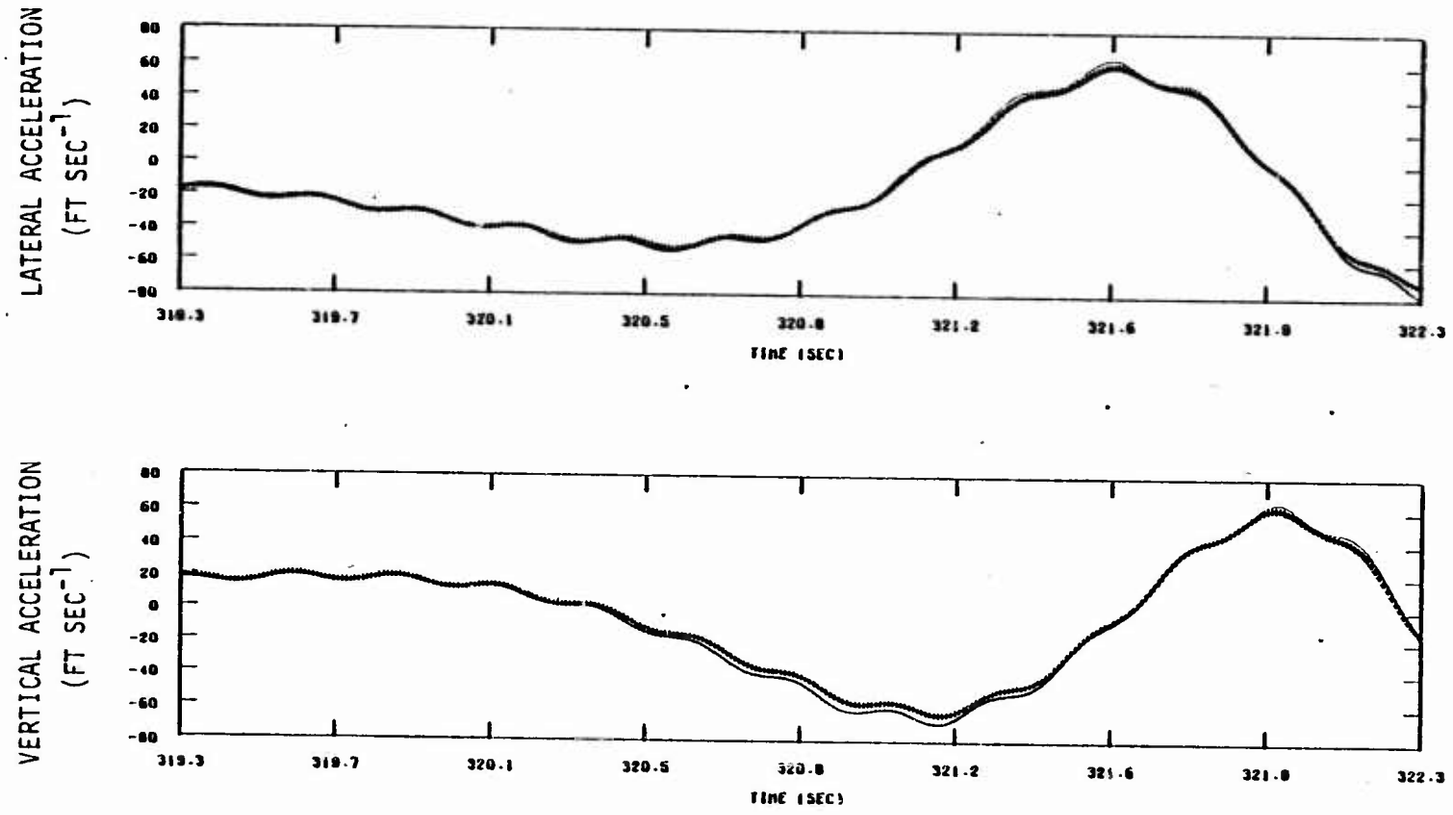

Figure 4.7 (Continued

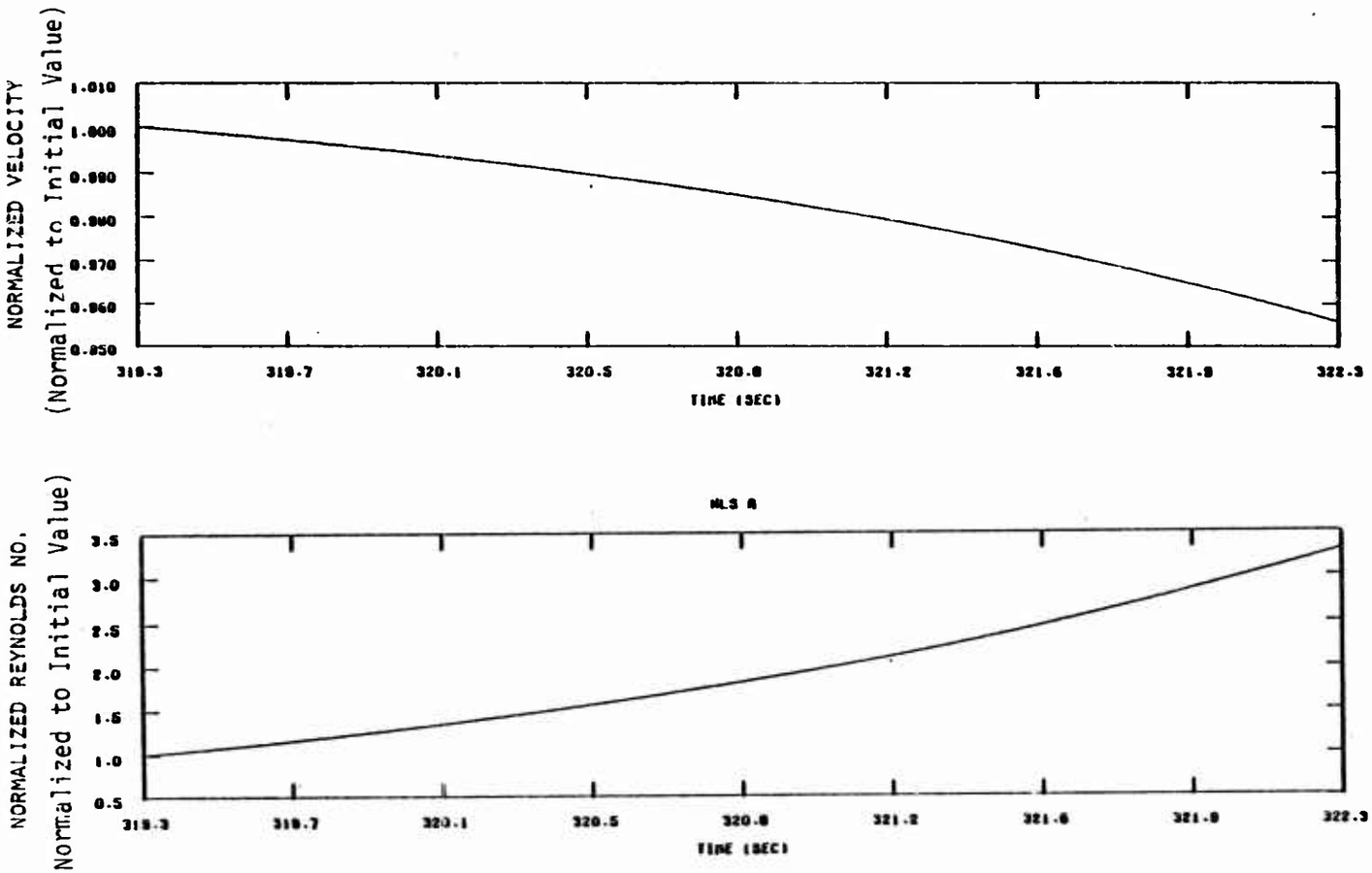

Figure 4.8 Normalized Velocity and Normalized Reynold's Number

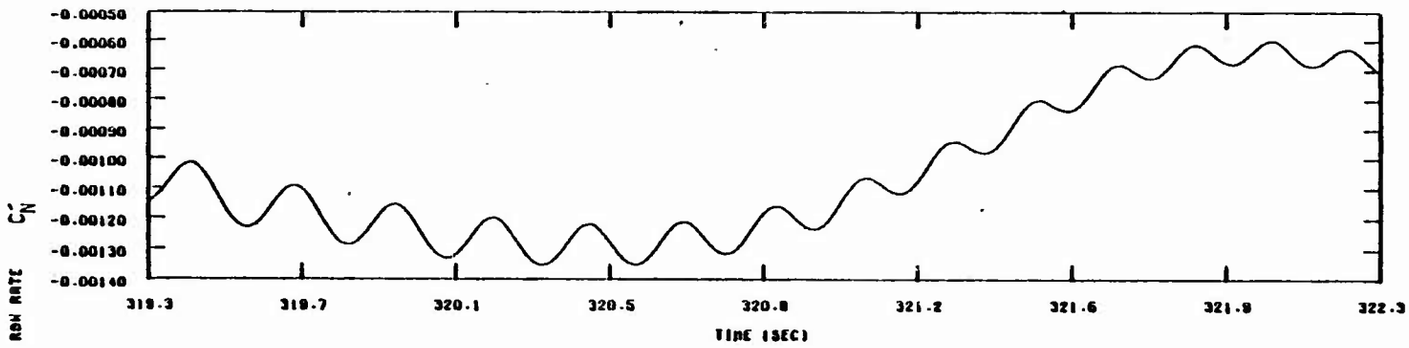

Figure 4.9 In-Plane Moment Used in Simulation

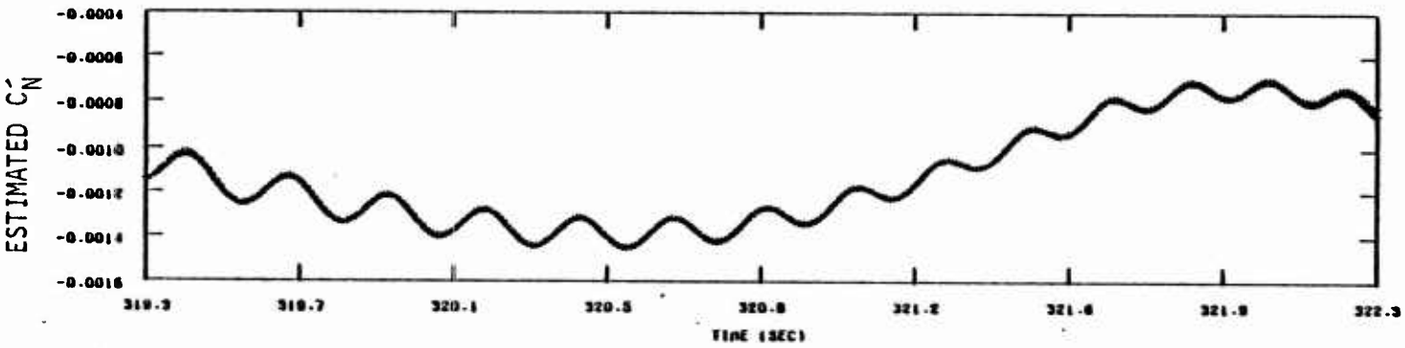

Figure 4.10 Estimate of In-Plane Moment and 2σ Bounds

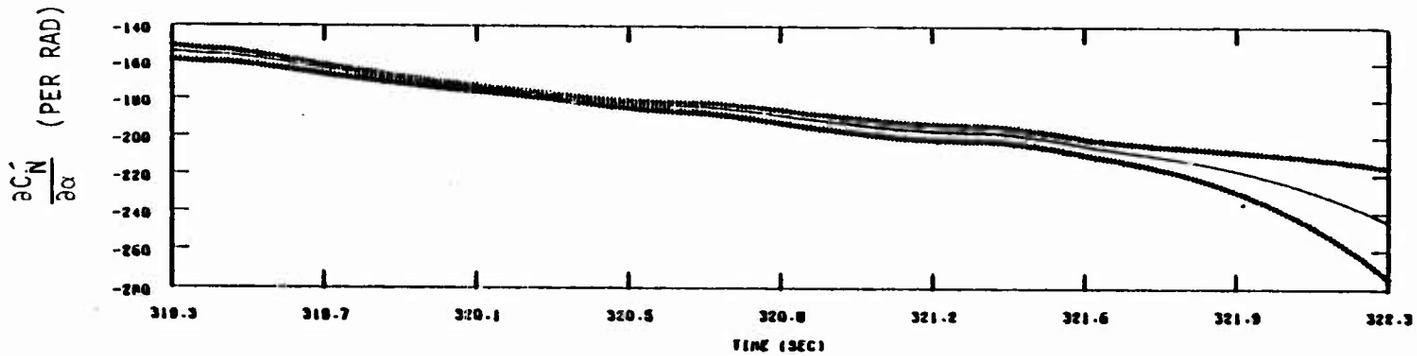

Figure 4.11 Estimated Stability Derivative of the In-Plane Moment (with 2σ Bounds)

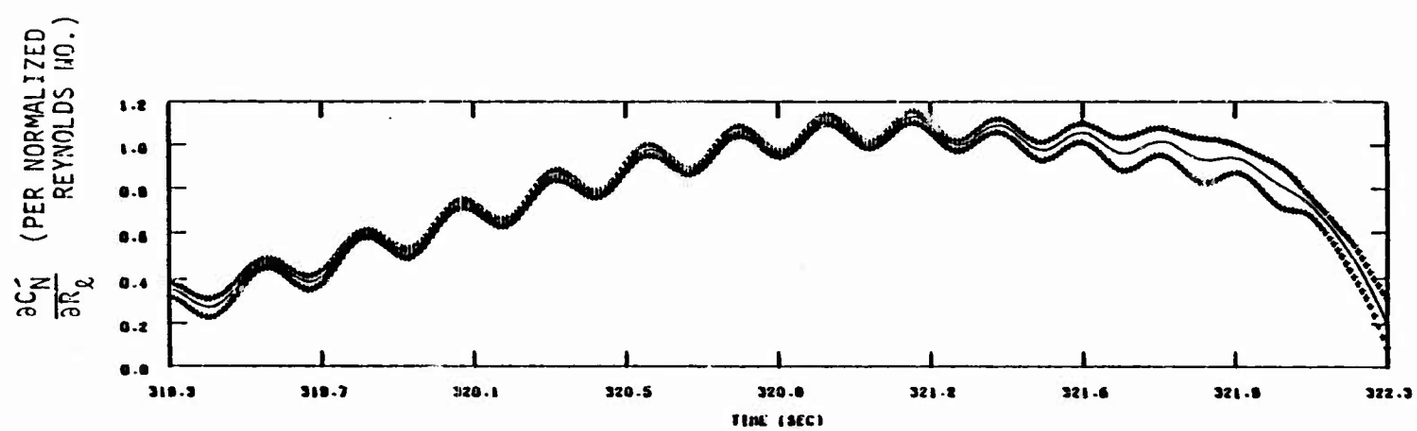

Figure 4.12 Variation of In-Plane Moment with Reynold's Number (with 2σ Bounds)

Figures 4.13 and 4.14 show the estimated in-plane force and its stability derivative with respect to angle-of-attack. The results are similar as for the aerodynamic moment coefficient.

The model structure (Tables 4.1 and 4.2) indicates that Reynolds number is quite important in explaining the variation of the in-plane moment, but what the stability derivatives (Figures 4.11 and 4.12) indicate is that the functional representation of Reynolds number effects is not adequate. Reynolds number is changing gradually, almost linearly, hence Reynolds number effects can probably be best modeled with a combination of regular polynomials and spline functions. When knots are taken close enough together, linear splines in time can be used to represent Reynolds number and Mach number effects (see Chapter V, Flight Data Processing).

4.5 SUMMARY

This chapter described an application of the integration system identification technology to a BRV simulation data. The application indicates briefly how this technology may be useful in isolating aerodynamic characteristics of BRV from a limited number of measurements and also verifies the software which implements the algorithms. Complex simulation aerodynamics can be modeled adequately by fairly simple functions. This chapter does not attempt to develop theories of the boundary layer transition phenomenon. Such an objective requires flight test data taken on the vehicles of interest. Analysis of the data from one particular vehicle for the specific purpose of developing a model of vehicle behavior during boundary layer transition is the subject of the following chapter.

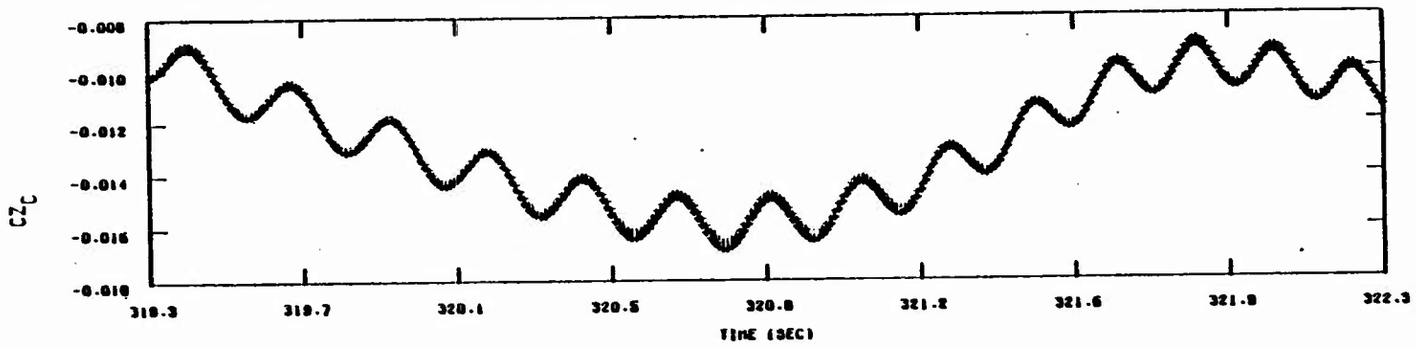

Figure 4.13 Estimate of In-Plane Force (with 2σ Bound)

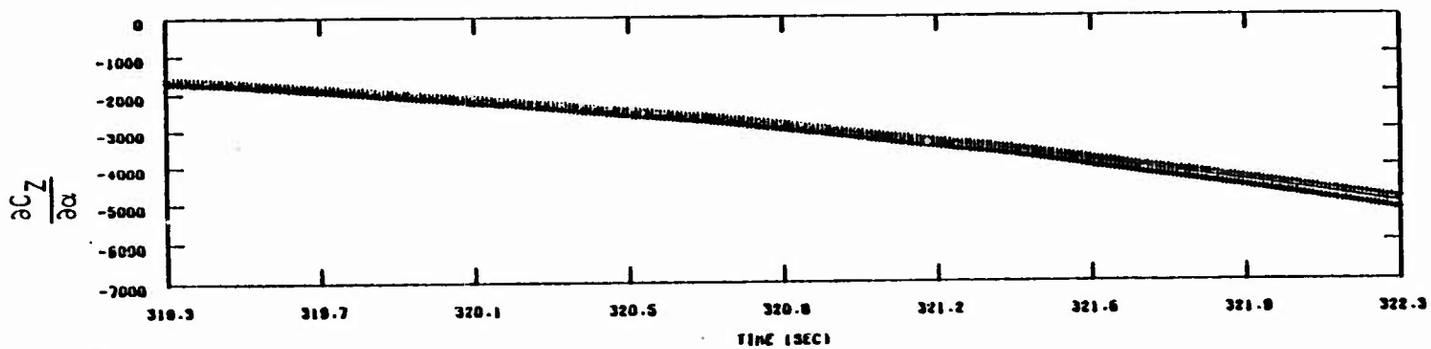

Figure 4.14 Estimate of Variation of In-Plane Force with Angle-of-Attack (with 2σ Bound)

CHAPTER V

FLIGHT DATA SYSTEM IDENTIFICATION RESULTS

5.1 INTRODUCTION

Previous chapters described ballistic reentry vehicle dynamic equations and showed how system identification techniques may be applied to estimate various unknown nonlinear force and moment coefficients in these equations based on limited time history data. This chapter describes the application of the techniques to a particular flight data.

The vehicle under consideration is a relatively blunt vehicle with a small cone angle. Reentry begins at a small angle-of-attack of 3°. Boundary layer transition starts at 90,000 ft altitude and is over at about 70,000 ft. Onboard measurements included 19 temperature, 1 acoustic, 2 vibration, and 3 axis angular rates and linear accelerometer measurements. In addition, a magnetometer measures roll rate. Altitude and total velocity are obtained either from off-board radar and optical measurements or from Kalman filter estimates of BET. Time history flight data at reentry is provided by SAMSO/Aerospace (ABRES) to SCI (Vt). The variables on the data tape are: (a) time, (b) altitude, (c) velocity, (d) dynamic pressure, (e) rate gyro (p,q,r,), (f) accelerometer (a_x, a_y, a_z), and (g) magnetometer roll rate.

Figures 5.1 and 5.2 show time histories of the accelerometer and rate gyro measurements. The measurements are noisy. The boundary layer transition starts after 320 sec. The oscillations produced during the BLT period damp out in about 4 sec.

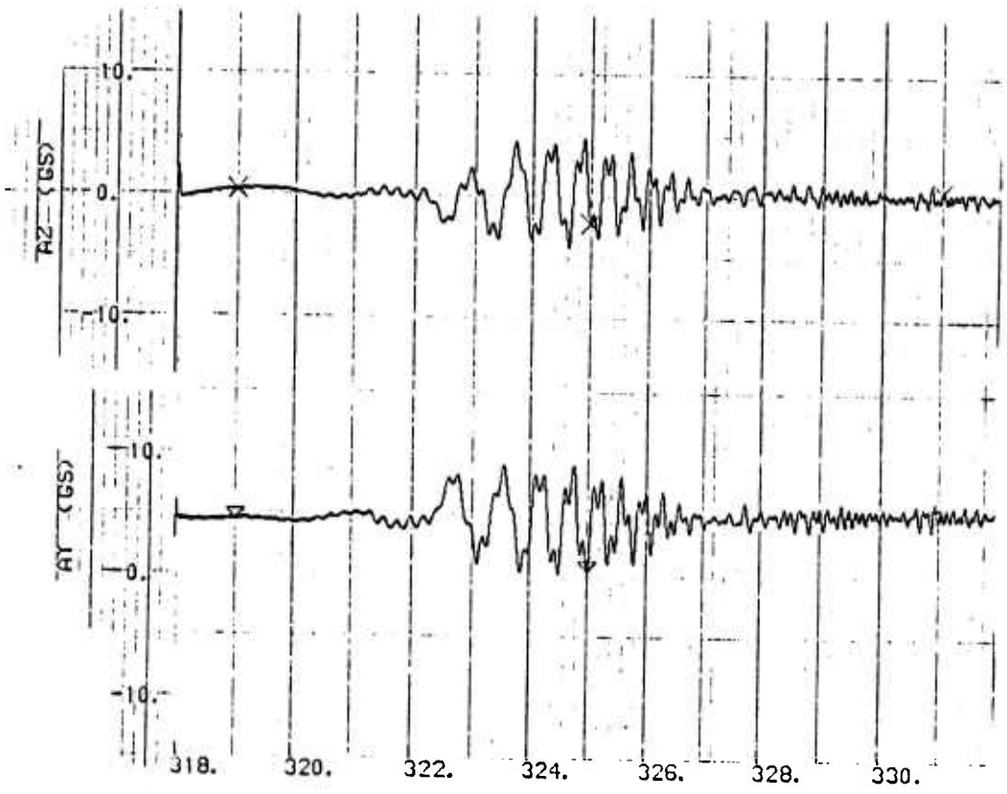

Figure 5.1 Flight Accelerometer Measurements

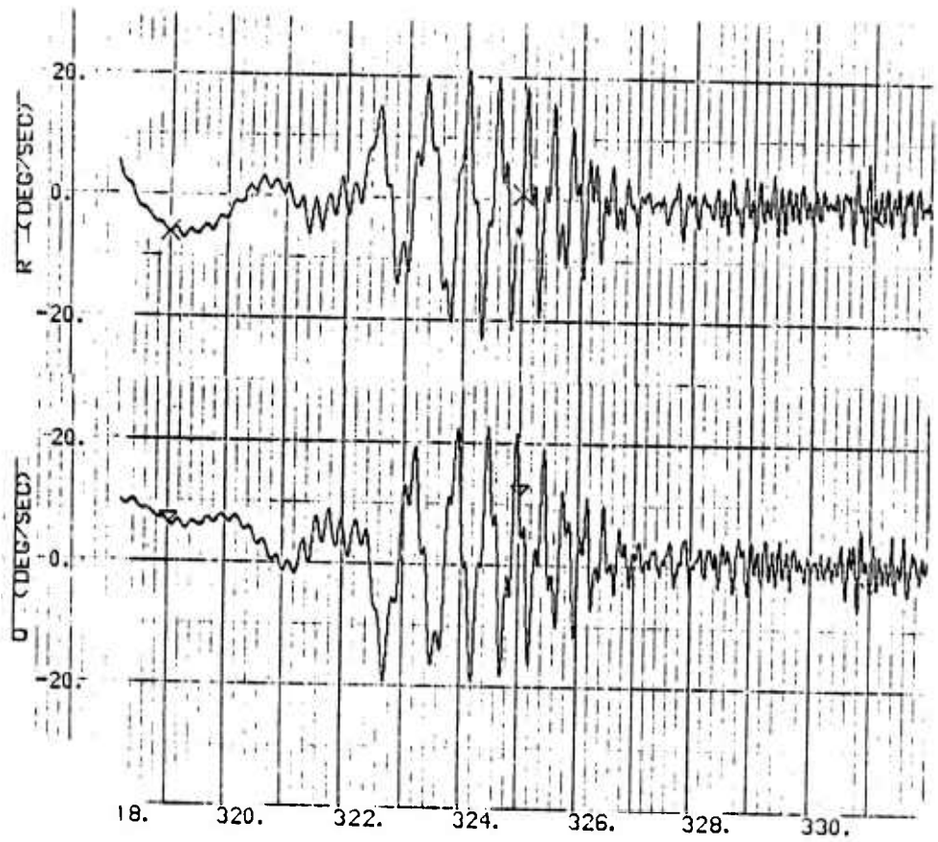

Figure 5.2 Flight Rate Gyro Measurements

5.2 DATA RECONSTRUCTION

The basic measurements used for identification are the body angular rates along the three principal axes (measured by gyros and magnetometer) and the body accelerations along the principal axes (measured by three body-fixed accelerometers). In addition, ground-based radars provide measurements of total speed and altitude. Data reconstruction procedures are described in Chapter III. It should be mentioned again that the reconstructed time histories are noisy and are used only in the model structure development stage. The maximum likelihood method develops filtered estimates of the time histories of these aerodynamic variables.

The aerodynamic variables of primary interest are:

(a) total angle-of-attack;
(b) windward meridian;
(c) windward meridian rate;
(d) total in-plane aerodynamic moment;
(e) total out-of-plane aerodynamic moment; and
(f) Reynolds number.

The ψ and θ are reconstructed starting from a zero value for ψ and θ at time 318.2 and propagating the kinematic angle equations (see Figures 5.3 and 5.4). The cross plot of θ and ψ is shown in Figure 5.5 (note the difference in scale on the x and y axes). Initially, the θ/ψ cross plots are close to circular. The windward meridian is estimated at time 318.875 using several methods (described in Chapter III) all of which give essentially the same results (see Chapter III). It was therefore concluded that the windward meridian estimate is quite good at the starting point.

Using this initial condition, Belknap's [22] method was used for reconstruction leading to the time histories shown in Figures 5.6 and 5.7. The reconstructed variables agree quite closely with those derived by AVCO [14]. Reconstructed in-plane and out-of-plane moments are shown in Figures 5.8 and 5.9.

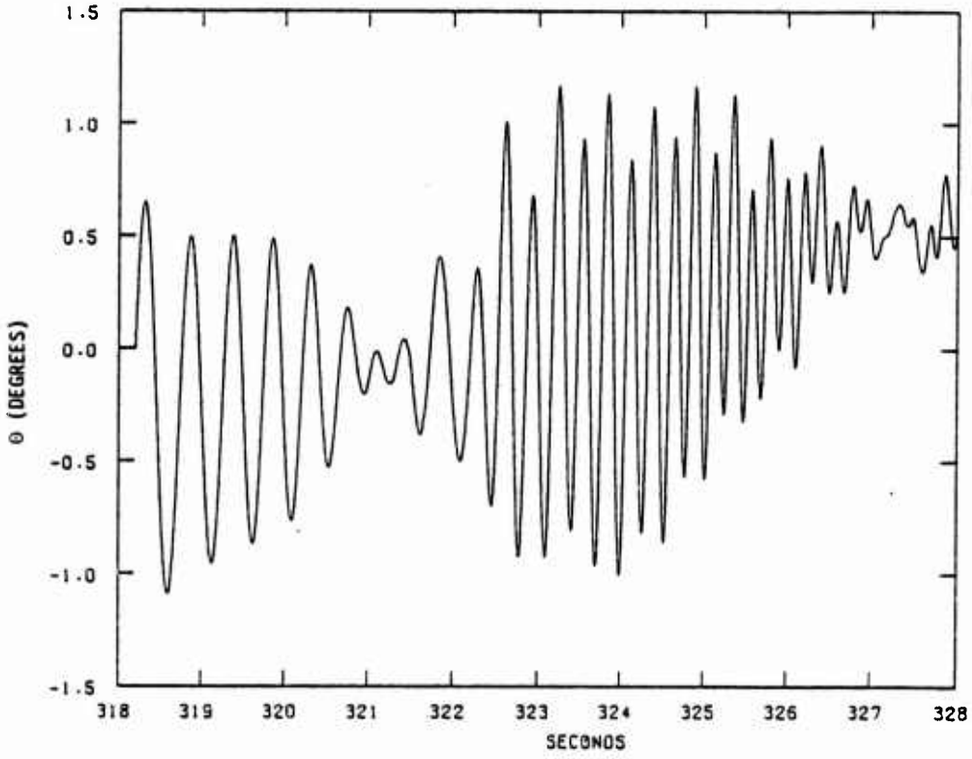

Figure 5.3 Pitch Angle Time History Obtained by Integration of Angular Rates

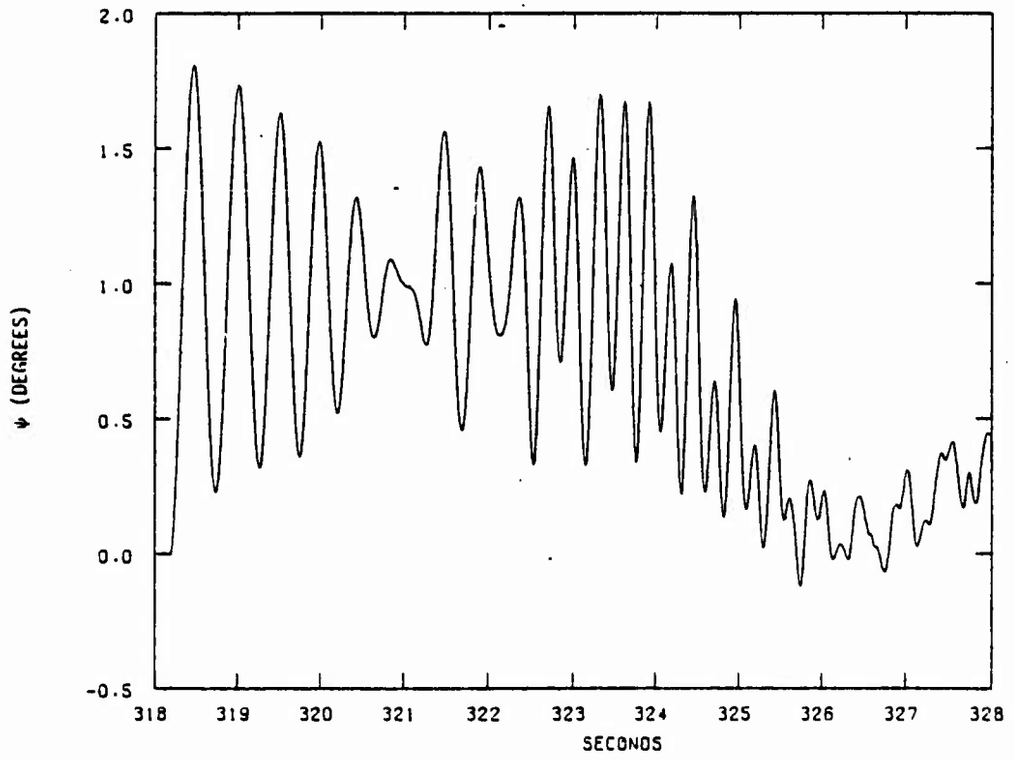

Figure 5.4 Yaw Angle Time History Obtained by Integration of Angular Rates

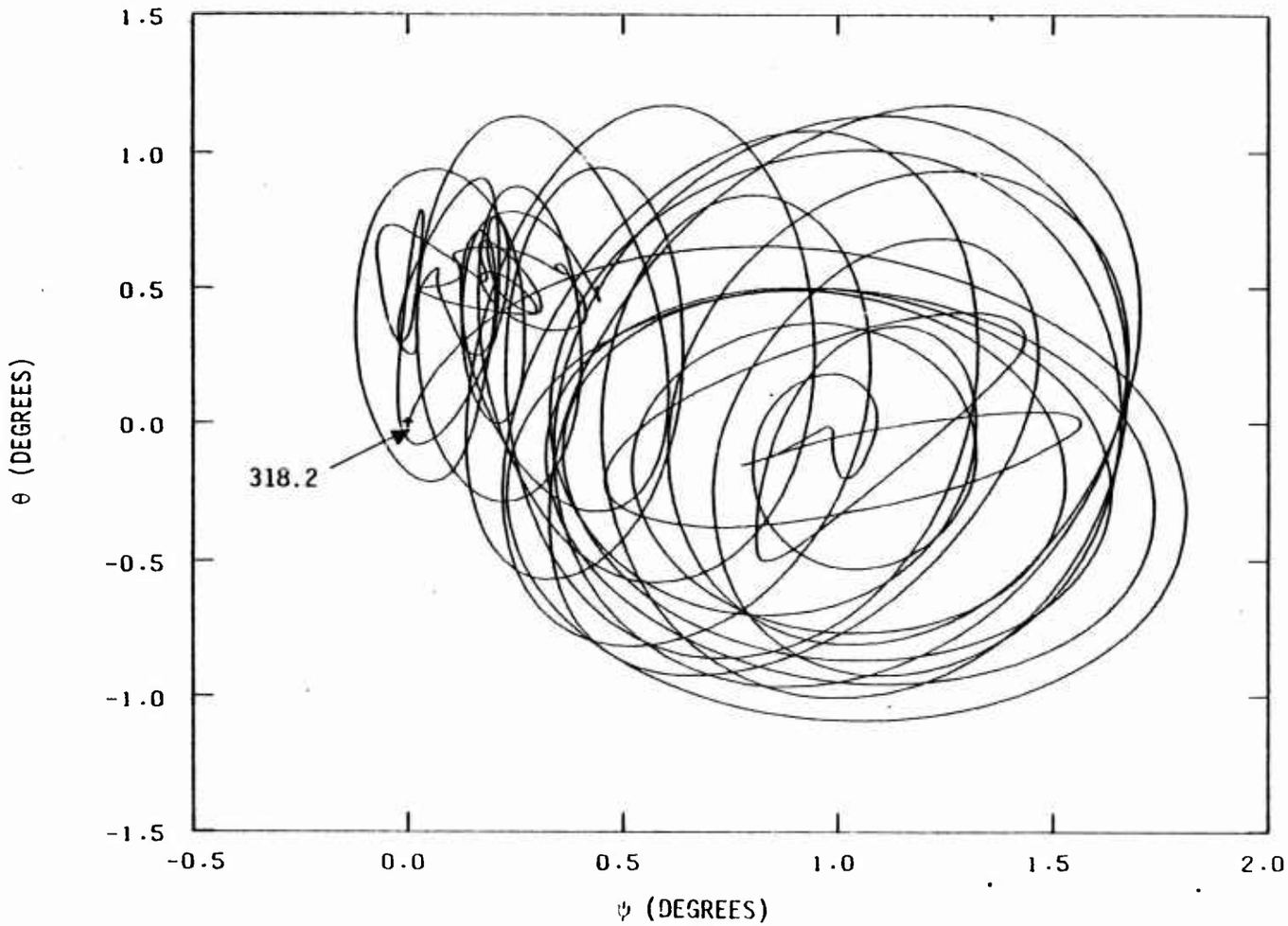

Figure 5.5 θ/ψ Cross Plot (Note Difference in Scale on x and y Axes)

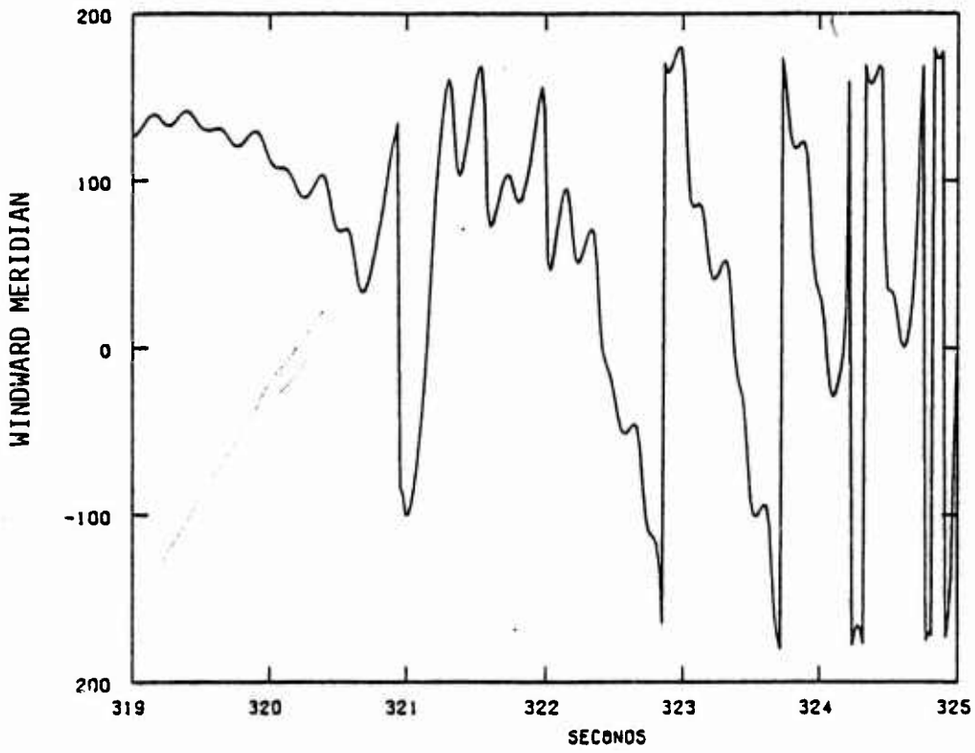

Figure 5.6 Reconstructed Windward Meridian

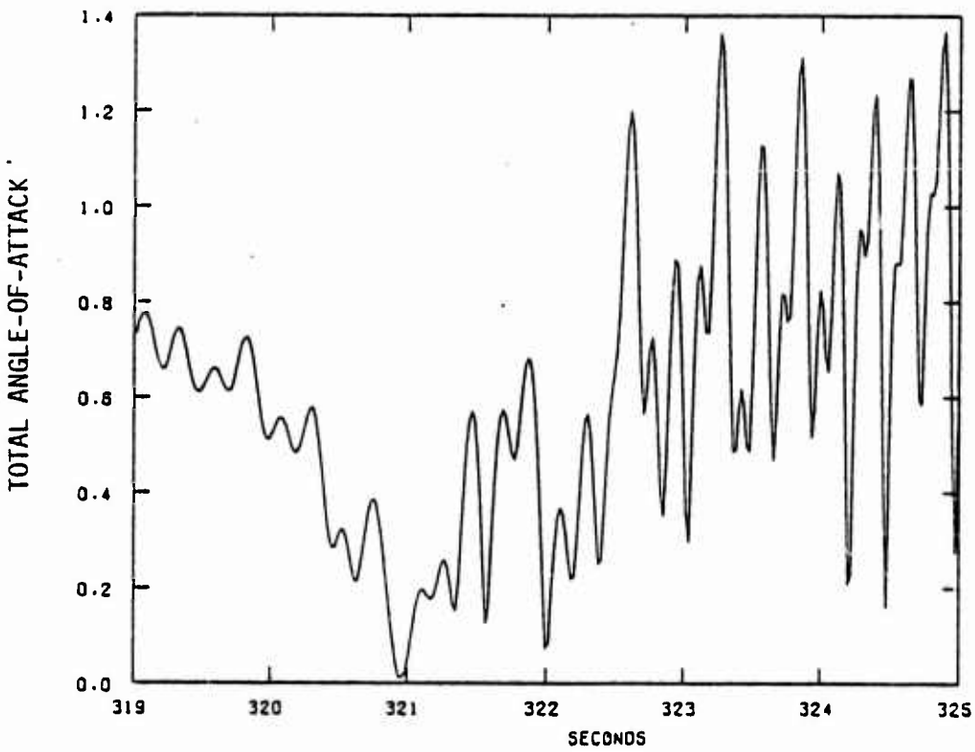

Figure 5.7 Reconstructed Total Angle-of-Attack

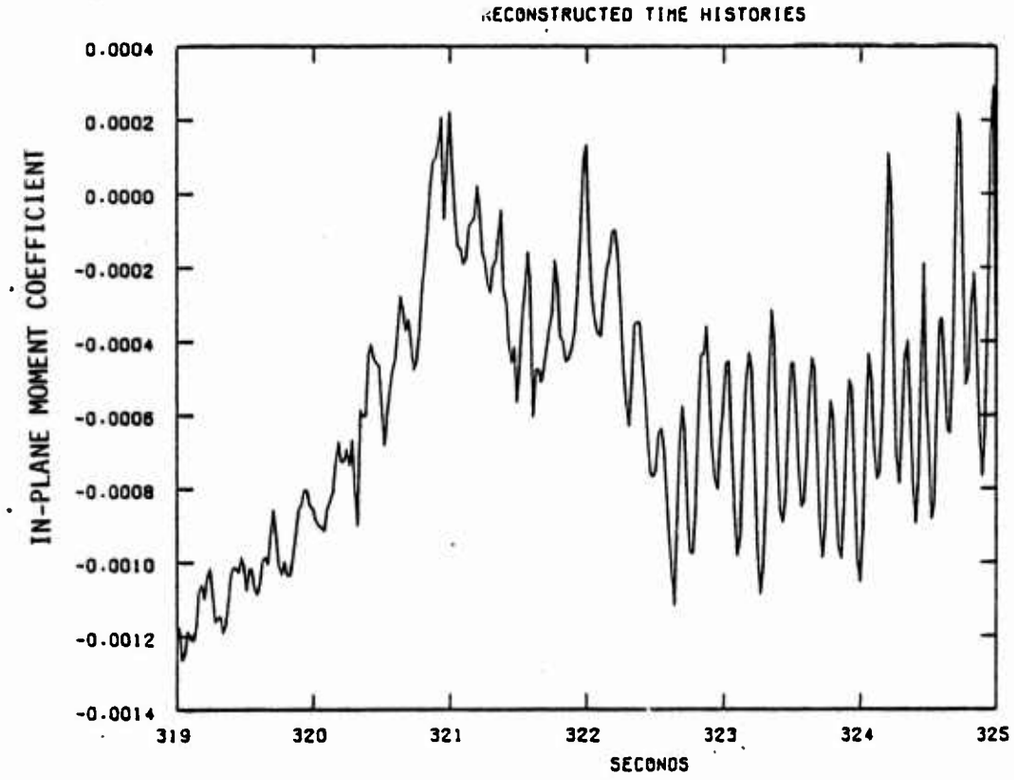

Figure 5.8 Reconstructed In-Plane Moment Coefficient

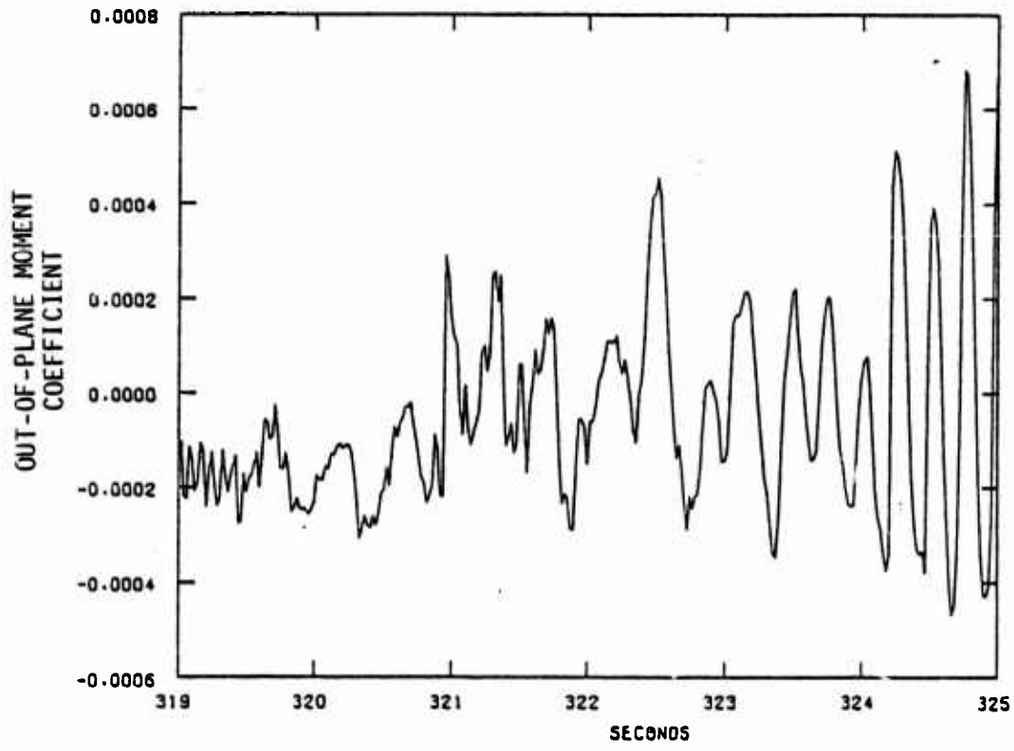

Figure 5.9 Reconstructed Out-of-Plane Moment Coefficient

5.3 MODEL STRUCTURE DEVELOPMENT

Development of physically meaningful model structures from the ballistic vehicle flight data is difficult because of the absence of good a priori information. AVCO studies[14] divide the in-plane moment into three parts: (1) inviscid moment, (2) a jump at the onset of BLT, and (3) an unexplained part. The unexplained part is quite large compared to the total in-plane moment. The out-of-plane moment was not modeled at all.

The following procedure is used for this effort. At boundary layer transition and just prior to and following boundary layer transition, significant changes in moments occur upon the ballistic reentry vehicle resulting from continuous or discontinuous changes in the aerodynamic parameters (e.g. the slope of the pitching moment vs. angle-of-attack curve). The approach used here is to apply statistical methods to determine the effects which are most significant in explaining the observed ballistic reentry vehicle time histories. These statistical methods are implemented in two model structure estimation programs, the optimal subset regression and globally optimum regression.

As a first step in studying the behavior of the ballistic vehicle, the in-plane moment from 318.75 sec to 322.0 sec is considered. Four possible variations are allowed:

(1) a sudden jump in C_N;
(2) a ramp change in C_N;
(3) a sudden jump in C_{N_α}; and
(4) a ramp change in C_{N_α}.

These variations are allowed at intervals of 0.25 sec. Using the optimal subset regression technique, the following model is obtained:

(1) C_{N_α} is constant at -0.527 rad^{-1};

(2) there is a ramp change in C_N of 0.000228 sec^{-1};

(3) there is a sudden jump in C_N of 0.000177 at 320.75; and

(4) there is a sudden jump in C_N of -0.000170 at 321.25.

The details of the model are given in Table 5.4. This simple model explains better than 96% variation in C_N. Figure 5.10

Table 5.4
Preliminary Model for C_N (318.875 - 322.0)

COEFFICIENT	VALUE	F-RATIO
Constant term	-0.000565	--
C_{N_α}	-0.0527	1223
Constant ramp in C_N	0.000228	627
Step in C_N at 320.75	0.000177	188
Step in C_N at 321.25	-0.000170	129

Variation explained: 96.3%
Overall F-ratio: 4000
Mean square C_N: .165E-06
Mean square prediction error = .62E-08
$\bar{\alpha} = \alpha - 0.24°$

shows the reconstructed C_N and C_N predicted by the model of Table 5.4. This is an excellent fit considering that there are significant errors during the reconstruction stage. The parameter estimates will improve in the maximum likelihood stage where the equations are not integrated open-loop.

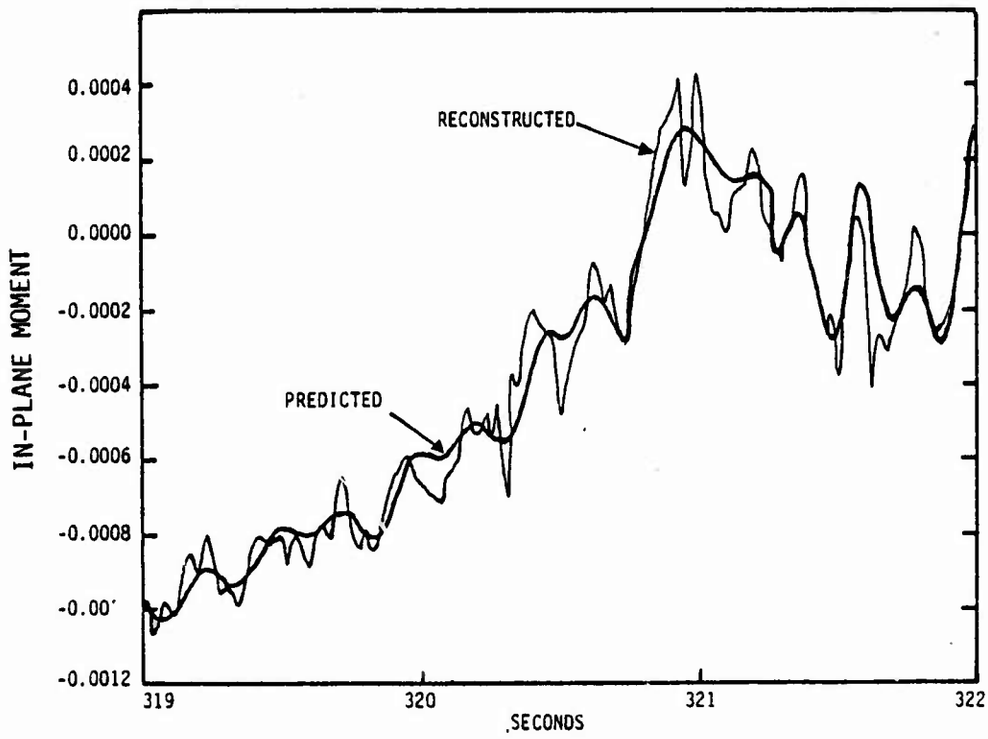

Figure 5.10 Reconstructed and Predicted Pitching Moment

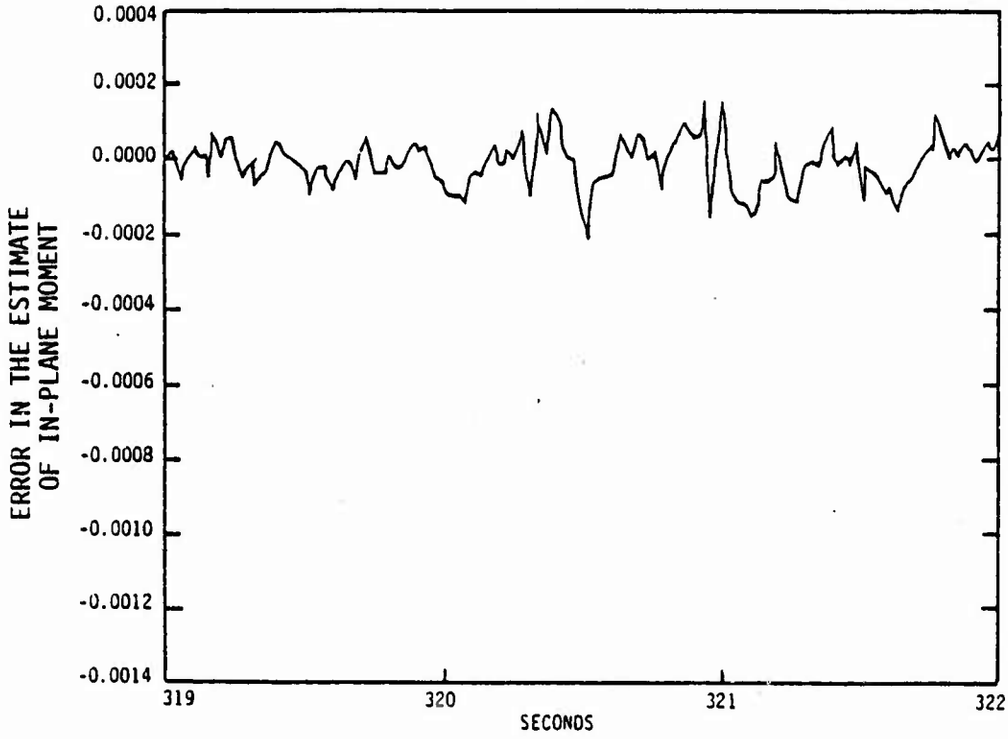

Figure 5.11 Error in the Prediction of Pitching Moment

The above calculation indicates that the in-plane moment acting at the vehicle c.g. may be related to certain aerodynamic variables quite satisfactorily. This provides a test of the algorithms on flight data and also shows that simple mathematical models may explain the seemingly complex behavior. Model structure estimation techniques are now applied to study two major theories of BLT.

5.3.1 Wind-Fixed Flow Sticking to the Body for Short Periods of Time

One of the hypotheses proposed for BLT is that the flow field around the ballistic reentry vehicle is basically wind-fixed. However, once a wind-fixed flow is established, it adheres to the body for a certain period of time. This occurs because at positive angle-of-attack, the transition front is asymmetric between the windward and the leeward sides of the vehicle; the transition is more advanced on the leeward side. If the windward meridian changes fast enough, however, the flow cannot re-establish instantaneously because of inertia, leading to asymmetries about the wind plane. This asymmetry would, then, explain the out-of-plane moment.

As shown in Chapter II, this mechanism converts the in-plane and out-of-plane moment components into two unknown functions $C_{m_w}(t)$ and $\varepsilon(\tau)$. This model would require relating $C_{m_w}(t)$ with angle-of-attack and Reynolds number (or time) and finding the function $\varepsilon(\tau)$, which may be dependent on t. This is a very complex estimation problem. To test the basis of this theory of BLT, however, the above formulation was simplified. The in-plane moment was set equal to C_{m_w} and the out-of-plane moment was modeled by a sum of discrete delays, i.e.,

$$C_N'(t) \approx C_{m_w}(t)$$

$$C_Z'(t) \approx \sum_{i=1}^{i_{max}} C_{m_w}(t-\tau_i)\ \varepsilon(t,\tau_i)\ \sin[\phi_w(t)-\phi_w(t-\tau_i)] \tag{5.1}$$

In addition, the time interval is divided into several regions and $\varepsilon(t,\tau_i)$ is assumed constant in each region, i.e.,

$$\varepsilon(t,\tau_i) = \varepsilon_j(\tau_i) \qquad t_j < t \leq t_{j+1} \qquad j = 1,2,\ldots,j_{max} \tag{5.2}$$

The problem now consists of two steps. In the first step, the in-plane moment is modeled using the total angle-of-attack and Reynolds number as independent variables. In the second step, the out-of-plane moment is related to lagged in-plane moment and the non-zero coefficients $\varepsilon_j(\tau_i)$ required to explain the out-of-plane moment are determined.

Model for the In-Plane Moment

The in-plane moment is primarily a function of angle-of-attack; however, the function may change with Reynolds number. In addition, sudden changes in the aerodynamic moment may result because of rapid changes in transition front over a portion of the body. All these effects are included in the maximal model specified for the regression program. The regression program chooses a subset of the maximal model which best explains the reconstructed moment using the fewest degrees of freedom. The subset is further refined using the globally optimum regression program.

Splines are used to model possible changes in C_{m_o} (the portion of in-plane moment independent of angle-of-attack) and

in C_{m_α} (the total angle-of-attack dependent portion of the in-plane moment). To model the in-plane moment from 318.875 sec to 323 sec, 15 knots are allowed at 318.875, 320.5, 320.8, 320.9, 321.0, 321.1, 321.2, 321.3, 321.4, 321.5, 321.75, 322.0, 322.25, 322.50 and 322.75. The maximal model then allows for jump and ramp changes in C_{m_o} and C_{m_α} at these locations. The optimal models for 2 through 10 variables in the equation are shown in Table 5.5. Just two terms, constant C_{m_o} and C_{m_α} can explain 69.3% of the variation in the in-plane moment and the addition of a jump in C_{m_α} at 320.8 increases the explained variation to 90.0%. Going from 4 to 5 variables, the jump in C_{m_α} at 320.8 is replaced by a ramp in C_{m_α} at 318.875 and a jump in C_{m_o} at 320.8. The procedure thereafter adds jumps in C_{m_o} at various time points until there are nine variables in the equation. The tenth variable is a jump in C_{m_α} at 322.75.

Figures 5.12 and 5.13 compare C_{m_o} estimates (as time functions) for different numbers of variables in the equation. The estimate changes significantly until there are five variables in the equation. Beyond that new terms fine tune the model. A similar behavior is observed for C_{m_α} estimate (Figures 5.14 and 5.15). It appears that models with fewer than five variables would not be physically acceptable. Models with 7, 8 or 11 parameters are considered most useful. A comparison of reconstructed in-plane moment and in-plane moment based on a seven-parameter model is shown in Figure 5.16. The error is also shown. Inclusion of more terms will improve the fit between the reconstructed time history and the model time history. Figure 5.17 shows the error about the inviscid moment versus angle-of-attack, and Figure 5.18 shows the total estimated in-plane moment versus angle-of-attack.

Table 5.5

Models for the In-Plane Moment

NO. OF VARIABLES	VARIABLE	VALUE	VARIATION EXPLAINED
2	C_{m_0}	0.0000714	59.3%
	C_{m_2}	-0.0778	
3	C_{m_0}	0.0000597	
	C_{m_2}	-0.0937	90.9%
	Jump in C_{m_2} at 320.8	0.0370	
4	C_{m_0}	0.0000381	
	C_{m_2}	-0.0916	92.6%
	Jump in C_{m_2} at 320.8	0.0463	
	Jump in C_{m_0} at 322.25	-0.000182	
5	C_{m_0}	-0.0000975	
	C_{m_2}	-0.0882	
	Ramp in C_{m_2} at 318.375 ...	0.0128	93.6%
	Jump in C_{m_0} at 320.8	0.000171	
	Jump in C_{m_0} at 322.25	-0.000252	
6	C_{m_0}	-0.000110	
	C_{m_2}	-0.0874	
	Ramp in C_{m_2} at 318.375 ...	0.0134	94.0%
	Jump in C_{m_0} at 320.8	0.000227	
	Jump in C_{m_0} at 321.0	-0.000122	
	Jump in C_{m_0} at 322.25	-0.000284	
7	C_{m_0}	-0.000103	
	C_{m_2}	-0.0883	
	Ramp in C_{m_2} at 318.875 ...	0.0135	
	Jump in C_{m_0} at 320.8	0.000271	94.2%
	Jump in C_{m_0} at 321.0	-0.000104	
	Jump in C_{m_0} at 322.0	-0.0000822	
	Jump in C_{m_0} at 322.25	-0.000218	
8	C_{m_0}	-0.0000912	
	C_{m_2}	-0.0889	
	Ramp in C_{m_2} at 318.875 ...	0.0128	
	Jump in C_{m_0} at 320.8	0.000263	94.8%
	Jump in C_{m_0} at 321.0	-0.000125	
	Jump in C_{m_0} at 321.75	0.000131	
	Jump in C_{m_0} at 322.0	-0.000182	
	Jump in C_{m_0} at 322.25	-0.000193	
9	C_{m_0}	-0.0000987	
	C_{m_2}	-0.0883	
	Ramp in C_{m_2} at 318.875 ...	0.0131	
	Jump in C_{m_0} at 320.8	0.000269	
	Jump in C_{m_0} at 321.0	-0.0000960	95.0%
	Jump in C_{m_0} at 321.5	-0.000103	
	Jump in C_{m_0} at 321.75	0.000193	
	Jump in C_{m_0} at 322.0	-0.000176	
	Jump in C_{m_2} at 322.25	-0.000207	
10	C_{m_0}	-0.0000971	
	C_{m_2}	-0.0888	
	Ramp in C_{m_2} at 318.875 ...	0.0135	
	Jump in C_{m_0} at 320.8	0.000267	
	Jump in C_{m_0} at 321.0	-0.0000975	95.2%
	Jump in C_{m_0} at 321.5	-0.000105	
	Jump in C_{m_0} at 321.75	0.000192	
	Jump in C_{m_0} at 322.0	-0.000174	
	Jump in C_{m_0} at 322.25	-0.000191	
	Jump in C_{m_2} at 322.75	-0.00631	

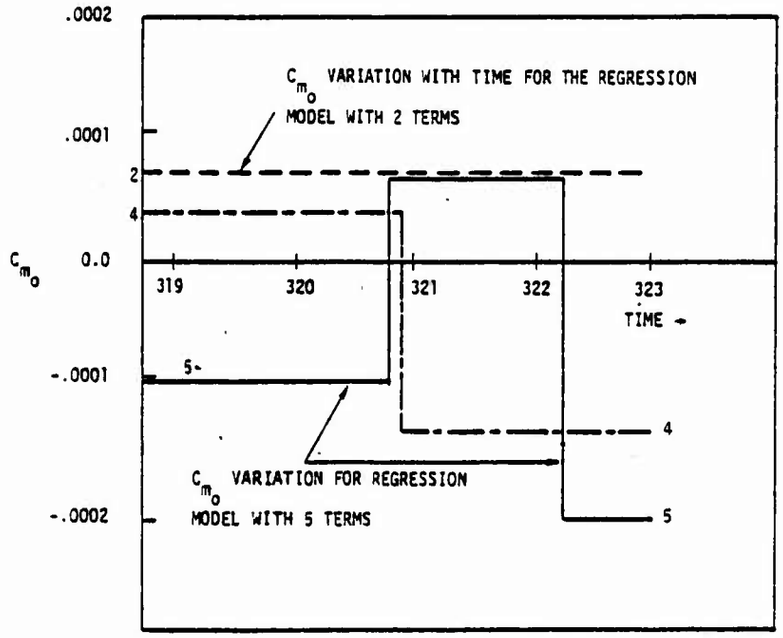

Figure 5.12 Estimated C_{m_o} for 2, 4, and 5 Terms in Regression Equation (Significant differences in these curves indicates that models with 2 or 4 terms cannot be believed.)

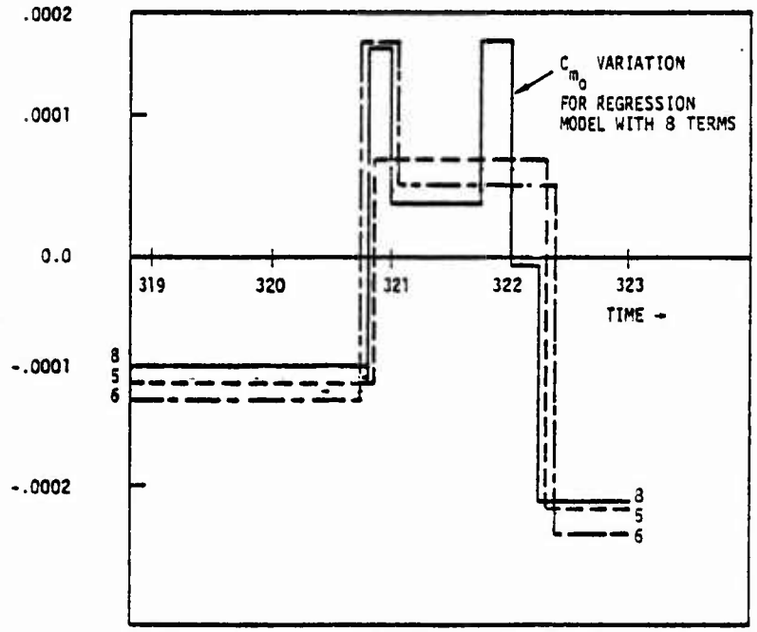

Figure 5.13 Estimated C_{m_o} for 5, 6, and 8 Terms in the Equation (Models with 5, 6, or 8 terms seem reasonable.)

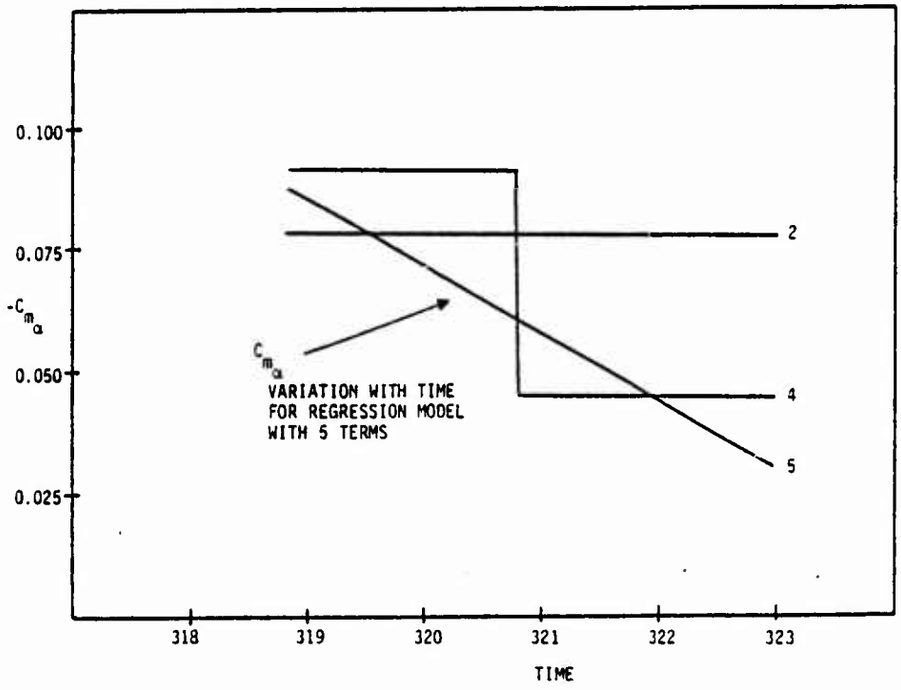

Figure 5.14 Estimated $C_{m\alpha}$ for 2, 4, and 5 Terms in the Equation (Significant differences in these curves indicates that models with 2 or 4 terms cannot be believed.)

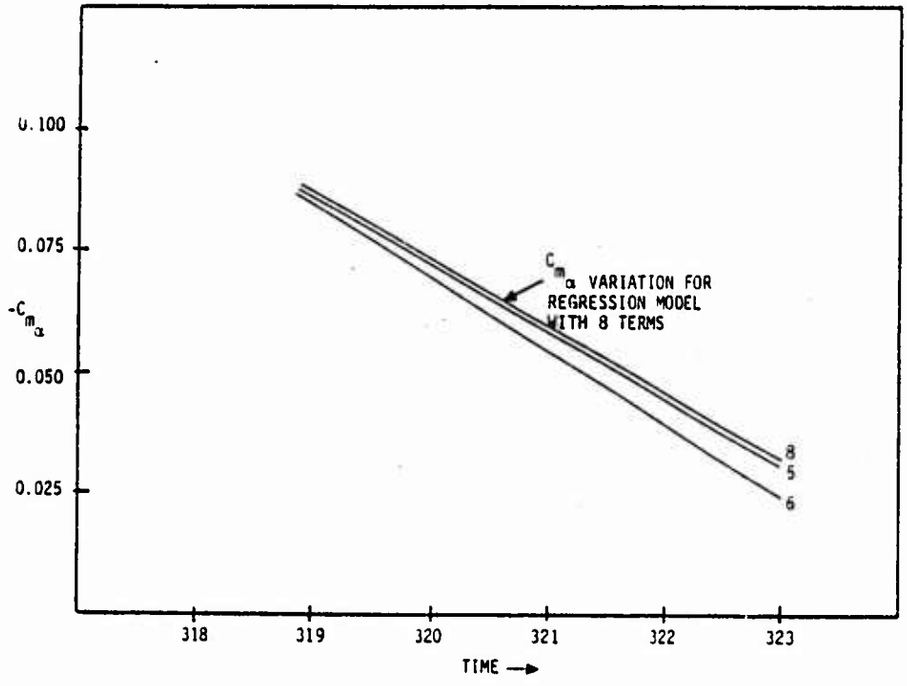

Figure 5.15 Estimated $C_{m\alpha}$ for 5, 6, and 8 Terms in the Equation (Models with 5, 6, or 8 terms seem reasonable.)

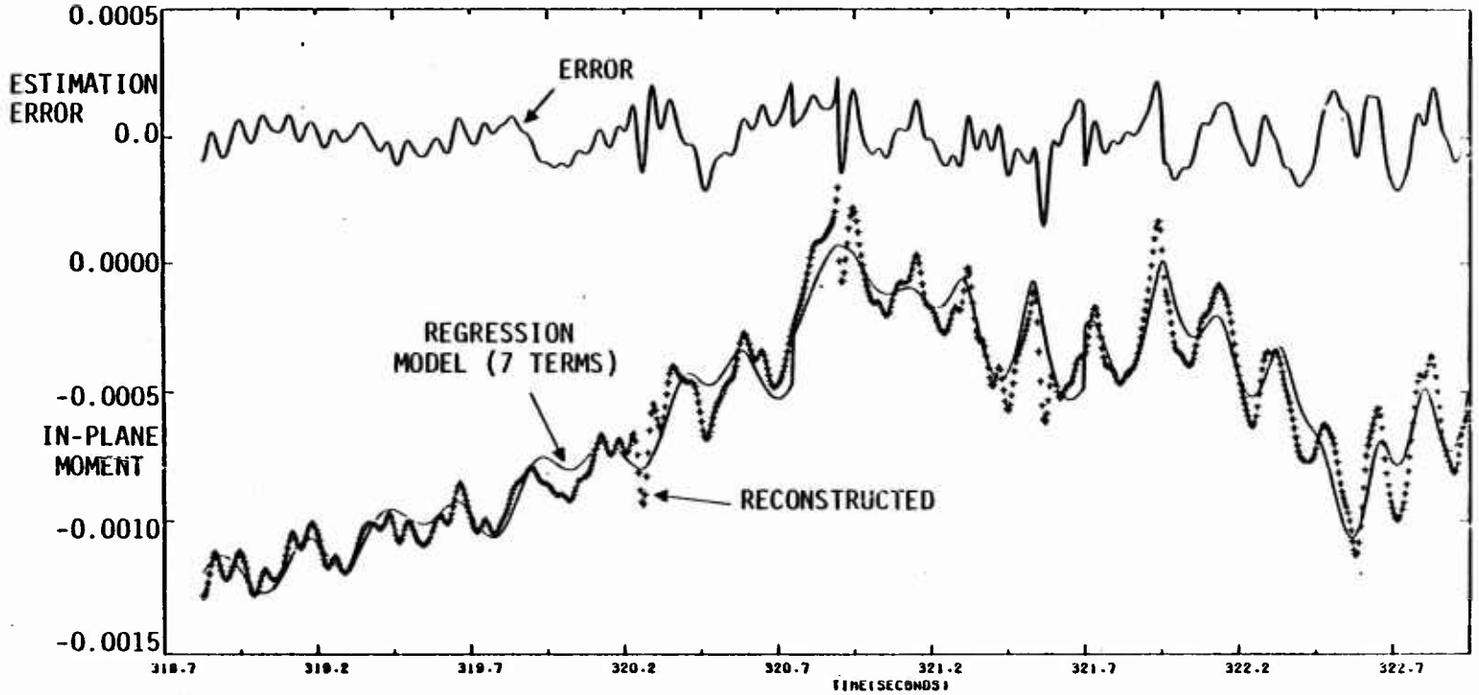

Figure 5.16 In-Plane Moment, Reconstructed and Estimated Based on Regression Model

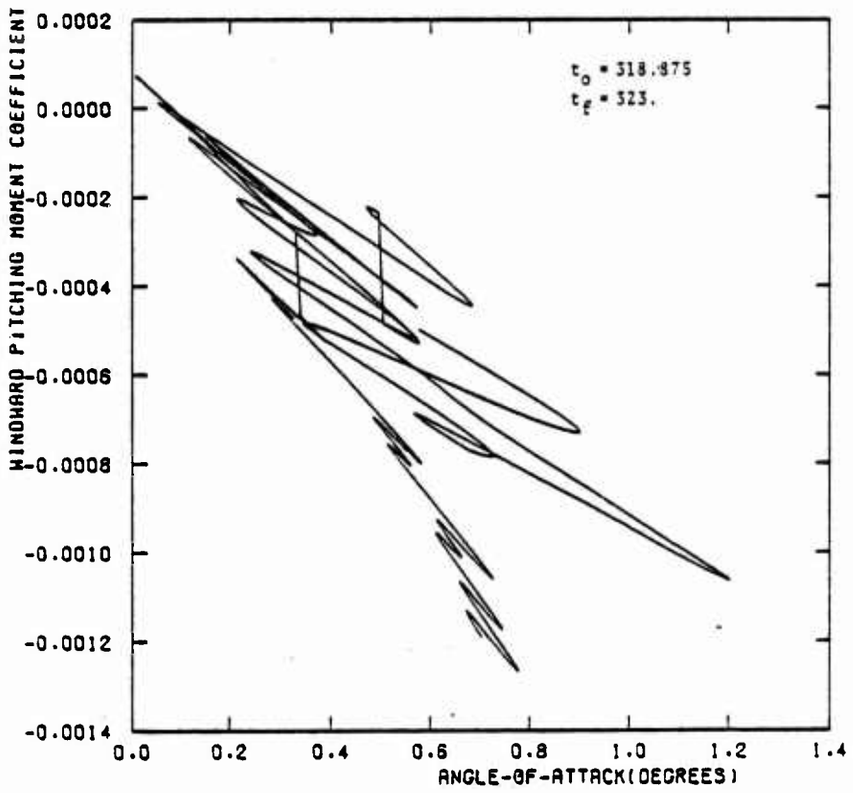

Figure 5.17 Total Estimated Windward Pitching Moment Coefficient

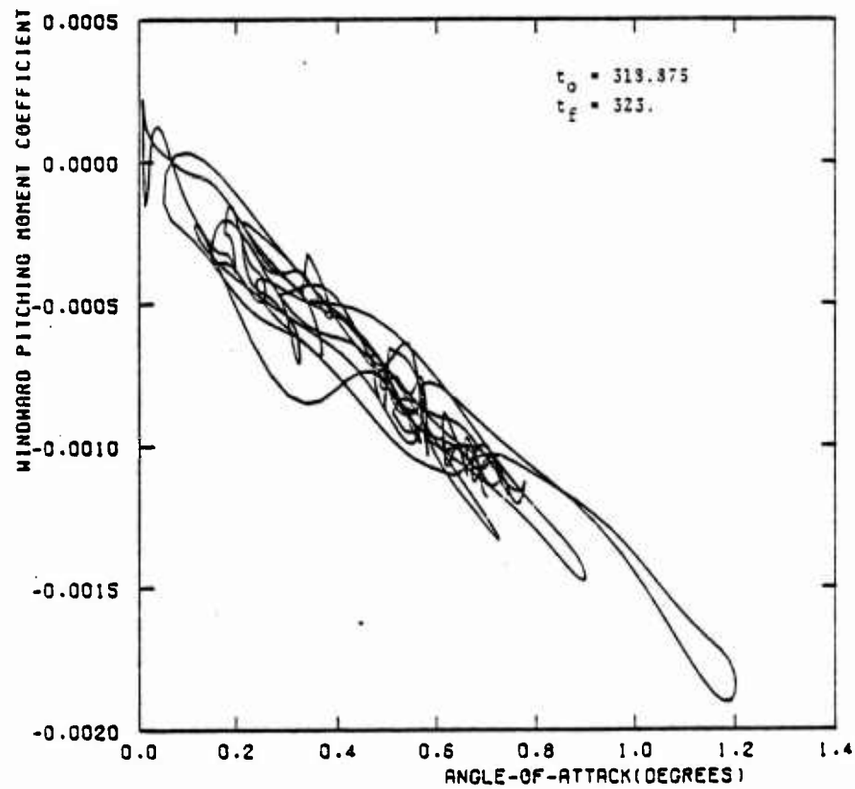

Figure 5.18 Error about the Windward Inviscid Pitching Moment Coefficient

Table 5.6 shows the F-value of various terms in models of different sizes. The F-value indicates the relative importance of a term in the regression equation. C_{m_α}, ramp in C_{m_α} at 318.875, and jumps in C_{m_o} at 321.8 and 322.25 are the most important variables. F-values also indicate accuracy with which these variables are estimated. (The standard deviation of estimating error on any parameter is related to its F-ratio, as (parameter value)/$\sqrt{\text{parameter F-ratio}}$.)

Table 5.6
Relative Importance of Terms in the In-Plane Model

COEFFICIENT	VALUE	STANDARD DEVIATION	F-VALUE
C_{N_o}	-0.000972		4110.
α	-0.0890	0.00139	779.
Ramp in C_{N_α} from 318.875	0.0138	0.000494	233.
Jump in C_N at 320.8	0.000178	0.0000116	521.
Ramp in C_N at 321.5	-0.000541	0.0000237	197.
Jump in C_N at 321.75	0.000245	0.0000174	103.
Ramp in C_N from 322.75	0.00125	0.000124	97.

Model for the Out-of-Plane Moment

Reconstructed out-of-plane moment is shown in Figure 5.19. As explained before, Eq. (5.1) is used to model the out-of-plane moment. Again, reconstructed moment from 318.875 to 323.0 sec is considered and regression methods are used to

select the best model with various numbers of parameters (see Table 5.7). The F-ratios of the parameters are shown in the brackets and the overall variation explained is indicated in the lower section of the table.

Table 5.7
Model for the Out-of-Plane Moment

PARAMETER	NUMBER OF PARAMETERS IN MODEL						
	2	3	4	5	6	7	8
Constant Term	-0.0000916	-0.0000882	-0.0000930	-0.0000949	-0.0000974	-0.0000987	-0.0000102
Delay of 0.2 sec at 320.75	0.186 (75)	0.627 (287)	0.479 (138)	0.480 (142)	0.481 (149)	0.531 (173)	0.360 (32)
Delay of 0.2 sec at 322.5		-0.590 (195)	-1.08 (203)	-1.06 (202)	-0.879 (124)	-0.880 (127)	-0.836 (146)
Delay of 0.2 sec at 322.25			0.640 (59)	0.504 (33)	0.340 (14)	0.298 (11)	
Delay of 0.125 sec at 322.25				0.158 (20)	0.349 (56)	0.642 (69)	0.048 (148)
Delay of 0.125 sec at 322.75					-0.278 (36)	-0.278 (38)	-0.201 (18)
Delay of 0.125 sec at 321.75						-0.291 (22)	-0.337 (30)
Delay of 0.2 sec at 321.0							0.284 (12)
Delay of 0.125 sec at 321.5							-0.631 (42.2)
VARIATION EXPLAINED:	8.3%	25.9%	30.9%	32.5%	35.4%	37.1%	40.1%

The model with three parameters has a constant term and two delay terms. The model implies that 0.627 fraction of the flow remains attached to the body of 0.2 sec starting at 320.75 TALO. At 322.5, 0.590 fraction of the flow stops remaining fixed to the body for 0.2 sec, leaving a fraction of 0.627-0.590 = 0.037, which still remains fixed to the body beyond 322.5. The one standard deviations on the estimated 0.520 and 0.590 values (using F-values of 287 and 195, respectively) are 0.037 and 0.042, respectively. The difference between the two values is, therefore, insignificant. We would

conclude form this model that the out-of-plane moment can be explained by a constant term and about 60% wind-fixed flow remaining attached to the body for about 0.2 sec between 320.75 and 322.5. As the model order is increased, the two prominant delays are 0.2 sec and 0.125 sec. The overall variation explained with 8 parameters is only 40.1%. This is because of the high level of noise in the reconstruction in-plane moment, out-of-plane moment and windward meridian.

The reconstructed out-of-plane moment is compared with the predicted out-of-plane moment based on the eight-parameter model in Figure 5.19. The error is quite random except it seems to be correlated with the angle-of-attack. This correlation could exist, for example, if the initial estimate of windward meridian were incorrect. Including the angle-of-attack in the regression

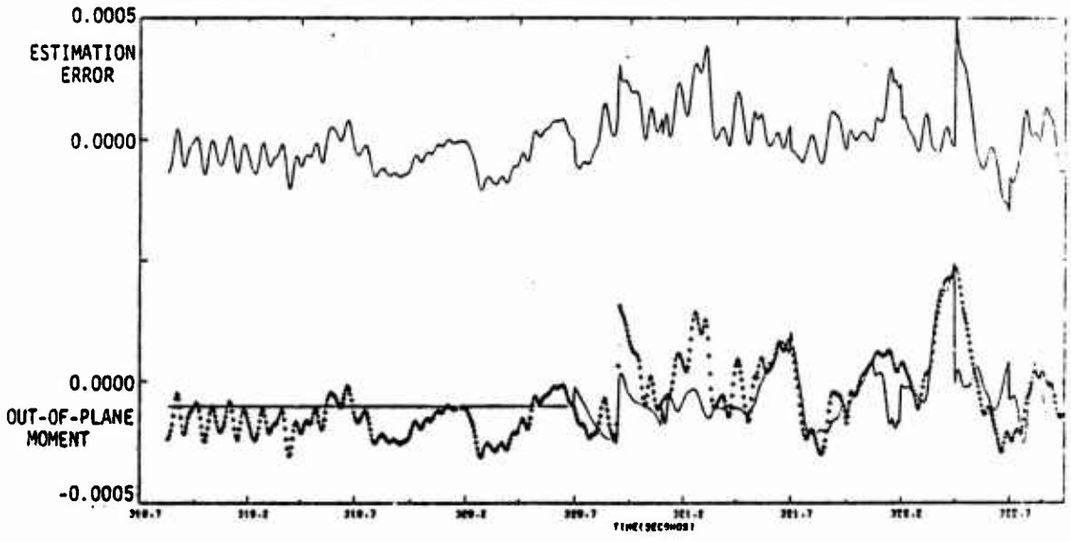

Figure 5.19 Reconstructed and Estimated Out-of-Plane Moment

variables gave results shown in Table 5.8. The best models with two or three parameters are the same as before. The

seven-parameter model can now explain a 51.8% variation in the out-of-plane moment. The overall nature of the model is the same, however, and the delay of 0.125 has been replaced by a delay of 0.15. The reconstructed and predicted out-of-plane moments based on the seven-parameter model of Table 5.8, are shown in Figure 5.20. The error looks random except for a few large peaks, caused probably by poor data.

Table 5.8
Model for the Out-of-Plane Model with Angle-of-Attack in Regression Equation

PARAMETER	NUMBER OF PARAMETERS IN THE MODEL					
	2	3	4	5	6	7
Constant Term	-0.0000916	-0.0000882	0.0000150	0.0000177	0.0000334	0.0000338
α			-0.0128 (128)	-0.0137 (159)	-0.0165 (257)	-0.0166 (271)
Delay of 0.2 sec at 320.75	0.186 (75)	0.627 (287)	0.658 (362)	0.587 (295)	0.527 (274)	0.583 (313)
Delay of 0.15 sec at 321.75						-0.310 (29)
Delay of 0.15 sec at 322.75				0.311 (73)	0.602 (213)	0.893 (175)
Delay of 0.2 sec at 322.5		-0.590 (195)	-0.536 (184)	-0.730 (273)	-0.571 (178)	-0.614 (206)
Delay of 0.15 sec at 322.75					-0.476 (147)	-0.467 (146)
VARIATION EXPLAINED:	8.3%	25.9%	35.9%	41.2%	50.1%	51.8%

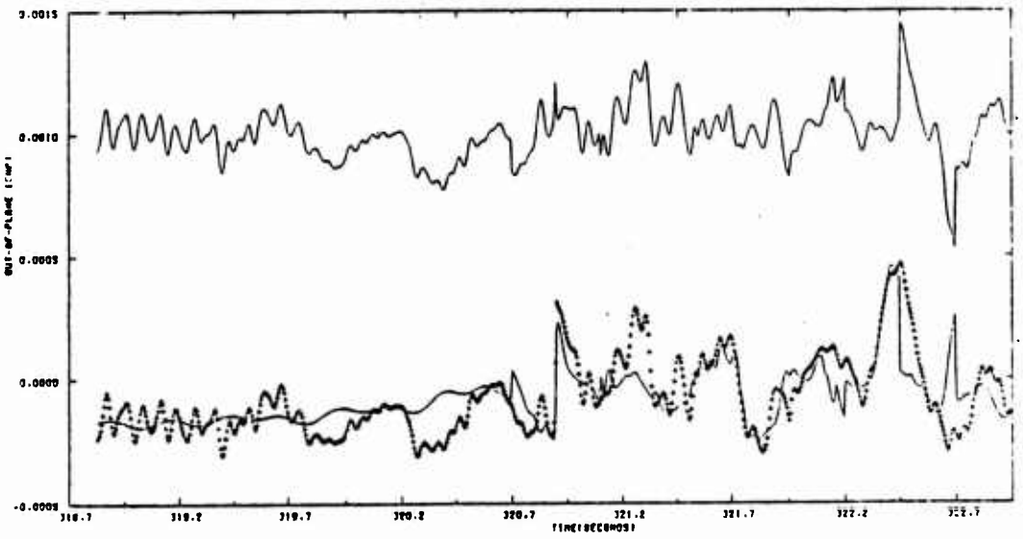

Figure 5.20 Reconstructed and Predicted Out-of-Plane Moment Based on Seven-Parameter Model of Table 5.7

5.3.2 Body-Fixed Irregularities Causing Asymmetric Flow

Let $C_{m_w}(t)$ be the aerodynamic moment caused by non-zero angle-of-attack. Suppose a body asymmetry at angle ϕ_b from the behicle y axis produces a body-fixed moment $C_b(t)$. Then the in-plane and the out-of-plane moments experienced by the vehicle are

$$C_N'(t) = C_{m_w}(t) + C_b(t) \cos[\phi_b - \phi_w(t)]$$

$$C_Z'(t) = C_b(t) \sin[\phi_b - \phi_w(t)]$$

The development of the model requires relating $C_{m_w}(t)$ to aerodynamic variables (e.g., angle-of-attack and Reynolds number) and finding $C_b(t)$ and ϕ_b. It will also be useful to relate $C_b(t)$ to some aerodynamic variables. Note that ϕ_b may change with time, though it should be constant over small intervals of time.

This problem is attempted in two steps. In the first step, $C_b(t)$ is eliminated from the above equations to give

$$C_N'(t) = C_{m_w}(t) + C_Z'(t) \operatorname{cotan}[\phi_b - \phi_w(t)]$$

Regression techniques are used to estimate a model for $C_{m_w}(t)$ and to estimate ϕ_b. $C_b(t)$ may then be obtained in the second step as

$$\hat{C}_b(t) = \sqrt{[C_N'(t) - \hat{C}_{m_w}(t)]^2 + [C_Z'(t)]^2}$$

where '^' denotes estimates. The correlation between $\hat{C}_b(t)$ and aerodynamic variables could be checked over the time history

if $C_b(t)$ is estimated. Regression methods used in model structure estimation indicate that this mechanism is highly unlikely.

Our analysis of body fixed moment causing dispersions during boundary layer transition is based on the assumption that the point on the body where the body fixed moment acts is fixed throughout the time. This contrasts with Cruschiel's analysis which assumed that both magnitude and location of the body fixed force is constant only over one cycle. Using our assumption, the regression analysis indicates that a completely body fixed moment is unlikely to explain the out-of-plane observed moments. This does not invalidate Cruschiel's results which used different assumptions. Future analysis should try to correlate the observations using Cruschiel's approximations.

5.4 SUMMARY

This chapter discusses the application of advanced system identification techniques to a set of flight data. The boundary layer transition region with its anomalous moments is analyzed. It appears that a wind-fixed flow sticking to the body for approximately 0.2 sec describes the BLT observed moments satisfactorily.

CHAPTER VI
SUMMARY

6.1 SUMMARY

This report develops a systematic procedure, based on system identification technology, for estimating mathematical models from ballistic reentry vehicle flight data. Accurate models resulting from such analysis will play a role in improving the overall accuracy of ballistic missile systems.

The system identification procedure, developed here, is general and, at least theoretically, extracts all available information from a set of data. The reconstruction step provides a reduced sensitivity to information limitation imposed by a certain fixed set of instruments, although it is recognized that additional instruments would provide more detailed models and enhance estimation accuracy. Any a priori information could also be used to advantage (none was available for this project). The model structure development step provides a means to test a large class of models. Therefore, this step is extremely useful in ballistic reentry vehicle flight data analysis, where a priori knowledge may be poor and one must resort to some amount of trial and error in the development of useful models. The model structure development phase is followed by the relatively sophisticated maximum likelihood parameter estimation stage. Here the model is fine tuned and the unknown parameters describing this model are accurately estimated, while taking into account possible errors in instruments. This overall structure divides the development of BRV mathematical models from flight test data into a series of simpler problems. In addition, it provides a flexible mechanism to handle a variety of situations in BRV flight data processing.

This structure is used to process a flight test data record and a simulation data record based on an advanced digital simulation [28]. Both simulation and flight test data records can be explained by relatively simple models.

Even such simple models are often hard to isolate using classical means because (1) it is necessary to recognize the stochastic effects and account for them, (2) instrument errors are important, and (3) automation of the model structure development stage allows quick comparison of thousands of both simple and complex models. The in-plane moment and force coefficients for the simulation data (without boundary layer transition) are explained adequately by just six terms and two terms, respectively. The model for the ballistic vehicle flight data during boundary layer transition is more complex, but the anomalous nature of the out-of-plane moment is explained by a wind-fixed flow remaining body fixed for about 0.2 sec during BLT. Better models may result from a more detailed simulation.

6.2 RECOMMENDATIONS

Though some significant conclusions may be drawn from this limited application of the techniques to one of the BRV flights, development of reliable, better detailed models will necessarily require extensive application of these techniques to a wide spectrum of ballistic vehicle flight data. Data from a single flight just does not contain the extent of information required for a detailed modeling, partly because good a priori information is unavailable. If the data is collected on several vehicles, it should be possible to more accurately correlate BLT mechanism with vehicle physical characteristics. This would provide an effective guide for future designs of ballistic reentry vehicles which would minimize impact dispersion resulting from the BLT phenomenon.

The significant modeling aspects of ballistic vehicles can be further improved by more detailed analysis of instrumentation requirements. Specialized techniques for such instrumentation specification have been developed [31] and can usefully be applied to such ballistic vehicle requirements.

APPENDIX A
ESTIMATION OF WINDWARD MERIDIAN ANGLE FROM ONBOARD SENSORS USING POLAR COORDINATES

Estimation of the location of the vehicle velocity vector is one of the first necessary tasks in reconstructing vehicle states from flight data. In the angular rate method, it is assumed that the center of the roughly circular path described by the reentry vehicle (RV) nose coincides with the velocity vector. To determine the path of the nose, the rate gyro measurements are integrated, using zero initial conditions, to determine vehicle pitch and yaw Euler angles. The mean values of the Euler angles over one or more cycles are then taken to locate the nominal velocity vector.

An alternate procedure for determining the velocity vector orientation and windward meridian angle is proposed here. Velocity orientation is determined from measurements at a single time point. This eliminates the need for rate measurements sufficient to allow integration over one cycle.

The procedure is based on two assumptions:

(1) Vehicle pitch and yaw angles about the nominal velocity vector orientation satisfy small angle linearity assumptions.

(2) Vehicle acceleration, as measured by the onboard accelerometers, lies in the wind plane.

Assumption (1) contributes very little error for the small angles of attack normally encountered (<3°). Assumption (2) is critical, but appears to be substantiated by previous flight data, except in regions of boundary layer transition (BLT). Therefore, this procedure, if it is to be used, should be applied to flight data prior to BLT.

Referring to Figure A.1, which shows a rear view of the RV looking along the velocity vector, the following definitions are made:

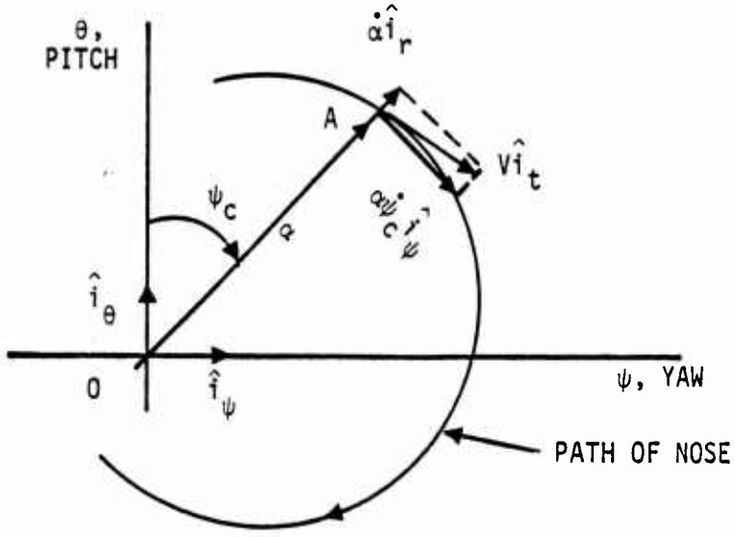

Figure A.1 Trajectory of Vehicle Nose

The vehicle translational velocity is assumed normal to the pitch-yaw plane and passes through the origin. Initial roll angle is assumed to be zero.

Five unit vectors are defined:

$\hat{i}_t$ - tangent to the path of the nose

$\hat{i}_{\psi_c}$ - traverse to the vector from the origin to nose position

$\hat{i}_r$ - radial along vector from origin to nose position

$\hat{i}_\theta$ - in direction of translation due to pitch (θ) rotation

$\hat{i}_\psi$ - in direction of translation due to yaw (ψ) rotation

Two angles are also defined:

ψ_c - classical precession angle relating wind plane OA to quasi-inertial axes ($\hat{i}_\theta$, $\hat{i}_\psi$)

α - total angle of attack between vehicle longitudinal axis and velocity vector

Based on Figure A.1, the following relationships are evident:

$$\bar{v} = v\hat{i}_t = \dot{\psi}\hat{i}_\psi + \dot{\theta}\hat{i}_\theta \tag{A.1}$$

$$= \alpha\dot{\psi}_c\hat{i}_{\psi_c} + \dot{\alpha}\hat{i}_r \tag{A.2}$$

where

$\bar{v}$ is the velocity of the nose (normalized by vehicle length).

The transformations between polar coordinates $\hat{i}_{\psi_c}$, $\hat{i}_r$ and rectangular coordinates $\hat{i}_\psi$, $\hat{i}_\theta$ are

$$\hat{i}_{\psi_c} = \cos\psi_c\hat{i}_\psi - \sin\psi_c\hat{i}_\theta \tag{A.3}$$

and

$$\hat{i}_r = \cos\psi_c\hat{i}_\theta + \sin\psi_c\hat{i}_\theta \tag{A.4}$$

Combining Eqs. (A.#) and (A.4) into A.2), letting c = cos and s = sin.

$$\bar{v} = [\alpha\dot{\psi}_c c\psi_c + \dot{\alpha}s\psi_c]\hat{i}_\psi + [-\alpha\dot{\psi}_c s\psi_c + \dot{\alpha}c\psi_c]\hat{i}_\theta \tag{A.5}$$

Comparing Eqs. (A.1) and (A.5).

$$\dot{\psi} = \alpha\dot{\psi}_c c\psi_c + \dot{\alpha}s\psi_c \tag{A.6}$$

$$\dot{\theta} = -\alpha\dot{\psi}_c s\psi_c + \dot{\alpha}c\psi_c \tag{A.7}$$

Using small angle assumptions

$$\dot{\psi} = qs\phi + rc\phi \tag{A.8}$$

$$\dot{\theta} = qc\phi - rs\phi \tag{A.9}$$

where the vehicle angular velocities are

q = pitch rate, r = yaw rate,

and where the vehicle roll angle is defined in Figure A.2.

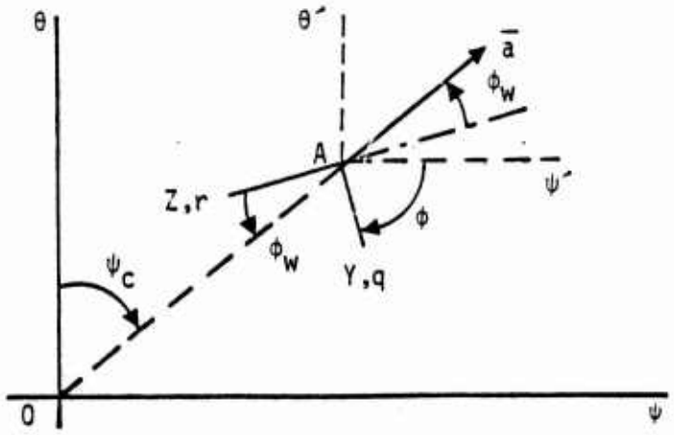

Figure A.2: Vehicle Roll and Windward Meridian Orientation

Again, it is assumed that the vehicle acceleration, $\bar{a}$, lies in the wind plane OA. Therefore,

$$\bar{a} = a_y \hat{i}_y + a_z \hat{i}_z \tag{A.10}$$

where a_y and a_z are measurements. From Figure 2, the windward meridian angle ϕ_w is

$$\phi_w = 180° + \tan^{-1} a_y/a_z \tag{A.11}$$

and the precession angle is

$$\psi_c = \phi - \phi_w \tag{A.12}$$

The roll angle ϕ is easily determined from roll rate measurements except for an arbitrary initial value.

As envisioned in the application of this procedure, the pitch-yaw axes are assumed initially coincident with the vehicle y-z axes.

Since ϕ_w is determined directly from onboard measurements and ϕ is assumed zero (or some arbitrary value), the precession angle ψ_c can be directly calculated using Eq. (A.12).

Using the assumed value of ϕ, the Euler rates $\dot{\phi}$, and $\dot{\psi}$ can be calculated from Eqs. (A.8) and (A.9). It remains to determine α and $\dot{\alpha}$.

If Eqs. (A.6) and (A.7) are squared and added, Eq. (A.13) results.

$$\begin{aligned}\dot{\psi}^2 + \dot{\theta}^2 &= \alpha^2\dot{\psi}_c^2 s^2\psi_c + \dot{\alpha}^2 s^2\psi_c + 2\alpha\dot{\alpha}\dot{\psi}_c s\psi_c c\psi_c \\ &\quad + \alpha^2\dot{\psi}_c^2 s^2\psi_c + \dot{\alpha}^2 c^2\psi_c - 2\alpha\dot{\alpha}s\psi_c c\psi_c \\ &= \alpha^2\dot{\psi}_c^2 + \dot{\alpha}^2 \qquad (A.13)\end{aligned}$$

But,

$$\begin{aligned}\dot{\psi}^2 + \dot{\theta}^2 &= (qc\phi - rs\phi)^2 + (qs\phi + rc\phi)^2 \\ &= q^2 + r^2 \qquad (A.14)\end{aligned}$$

where q and r are measured quantities. Therefore,

$$q^2 + r^2 = \alpha^2\dot{\psi}_c^2 + \dot{\alpha}^2 \qquad (A.15)$$

Now, $\dot{\psi}_c$ in Eq. (A.15) is

$$\begin{aligned}\dot{\psi}_c &= \dot{\phi} - \dot{\phi}_w \\ &\cong p - \dot{\phi}_w \qquad (A.16)\end{aligned}$$

where $\dot{\phi}_w$ can be determined numerically from successive measurements of vehicle accelerations using Eq. (A.11), and p is the measured roll rate.

Another equation in addition to Eq. (A.15) is necessary to find α and $\dot{\alpha}$. Multiplying Eq. (A.6) by $s\psi_c$ and Eq. (A.7) by $c\psi_c$, and adding yields

$$\dot{\psi}_s s\psi_c + \dot{\theta}_c c\psi_c = \dot{\alpha} \tag{A.17}$$

which can be used in Eq. (A.15) to yield

$$\alpha = \sqrt{\frac{q^2 + r^2 - \dot{\alpha}^2}{\dot{\psi}_c^2}} \tag{A.18}$$

The pitch and yaw angles can now be determined

$$\theta = \alpha c\psi_c \tag{A.19}$$

$$\psi = \alpha s\psi_c \tag{A.20}$$

The initial vehicle velocities can also be estimated by

$$u = V \tag{A.21}$$

$$v = -V\psi \tag{A.22}$$

$$w = V\theta \tag{A.23}$$

APPENDIX B

MEASUREMENT EQUATIONS

This appendix gives the equations for measurements, taken during a ballistic reentry vehicle flight, in terms of the equations of motion state variables, instrument errors, and other related terms.

Equations for six on-board instrument outputs are:

(1) Axial Accelerometer

$$a_A = \dot{u} - vr + wq + (q^2 + r^2)x_{cg} + (pq - \dot{r})y_{cg} + (pr + \dot{q})z_{cg} + b_{a_A}$$

(2) Lateral Accelerometer

$$a_L = \dot{v} - wp + ur + (pq + \dot{r})x_{cg} - (r^2 + p^2)y_{cg} + (rq - \dot{p})z_{cg} + b_{a_L}$$

(3) Vertical Accelerometer

$$a_V = \dot{w} - uq + vp + (pr - \dot{q})x_{cg} + (rp + \dot{p})y_{cg} + (q^2 + p^2)z_{cg} + b_{a_V}$$

(4) Roll Rate

$$p_m = p + b_p$$

(5) Pitch Rate

$$q_m = q + b_q$$

(6) Yaw Rate

$$r_m = r + b_r$$

Off-board measurements include radar and optical cameras. Outputs of these instruments are one or more of the following:

(1) Altitude

$$h_m = -Z_E + b_h$$

(2) Range

$$R_m = (1 + k_R)(X_E^2 + Y_E^2 + Z_E^2)^{1/2} + b_R$$

(3) Azimuth Angle

$$\psi_e = (1 + k_{\psi_E}) \tan^{-1} (X_E/Y_E) + b_{\psi_E}$$

(4) Elevation Angle

$$\gamma_e = (1 + k_{\gamma_E}) \tan^{-1} \frac{Z_E}{(X_E^2 + Y_E^2)^{1/2}} + b_{\gamma_E}$$

(5) Range Rate

$$\dot{R} = (1 + k_{\dot{R}}) \frac{Y_E\dot{X}_E + Y_E\dot{Y}_E + Z_E\dot{Z}_E}{(X_E^2 + Y_E^2 + Z_E^2)^{1/2}} + b_{\dot{R}_m}$$

REFERENCES

1. Hall, W.E. and Gupta, N.K., "System Identification for Nonlinear Flight Regimes," AIAA Journal of Spacecraft and Rockets, Vol. 14, No. 2, pp. 73-80, February 1977.

2. Nelson, R.L., "The Motions of Rolling Symmetrical Missiles Referred to a Body-Axis System," National Advisory Committee for Aeronautics, Technical Note 3737, November 1956.

3. Chrusciel, G.T., "Analysis of R/V Behavior During Boundary Layer Transition," Lockheed TM-81-11/80, December 1973.

4. Lusardi, R.J., Nicolaides, J.D., Ingram, C.W., "Determination of Nonsymmetric Aerodynamics of Re-entry Missiles," Journal of Spacecraft and Rockets, April 1975.

5. Platus, D.H., "Angle-of-Attack Control of Spinning Missiles," Journal of Spacecraft and Rockets, Vol. 12, No. 4, 1974.

6. Vaughn, H.R., "A Detailed Development of the Tricyclic Theory," Sandia Laboratory, Albuquerque, N.M., SC-M-67-2933, February 1968.

7. Barbera, F.J., "An Analytical Technique for Studying the Anomalous Roll Behavior of Re-entry Vehicles," Journal of Spacecraft and Rockets, November 1969.

8. Chrusciel, G.T., "Effect of RV Lift on Performance During Boundary Layer Transition," Lockheed TM 81-11/120, August 1975.

9. Chrusciel, G.T., "Three Degree of Freedom Hypersonic Wind Tunnel Results Employing Onboard Rate Gyros - I Asymmetric Body," Lockheed IDC 81-11/2590. Presented as AIAA Paper 76-94, January 1976.

10. Martellucci, A., Neff, R.S., "Influence of Asymmetric Transition on Re-entry Vehicle Characteristics," Journal of Spacecraft and Rockets, May 1971.

11. Waterfall, A.P., "Effect of Ablation on the Dynamics of Spinning Re-entry Vehicles," Journal of Spacecraft and Rockets, September 1969.

12. Hodapp, A.E., Jr., "Effects of Unsymmetrical Stability Derivative Characteristics on Re-entry Vehicle Transient Angular Motion," Journal of Spacecraft and Rockets, February 1976.

13. Hodapp, A.E., Jr., "Effects of Unsymmetrical Stability Derivative Characteristics on Re-entry Vehicle Trim Angle Behavior," Journal of Spacecraft, May 1974.

14. AVCO Transition Divergence Analysis (U), AS-76-05357, December 2, 1976, Classified.

15. King, H.H., "Turbulence Wedge Phenomenas Soucre of Trajectory Dispersion During Boundary Layer Transition," Briefing Slides, Effects Technology, Inc., November 4, 1976.

16. Hall, W.E., Gupta, N.K., Smith, R., "Identification of Aircraft Stability and Control Coefficients for the High-Angle-of-Attack Regime," Technical Report No. 2, Systems Control, Inc., Engineering Report to the Office of Naval Research on Contract N00014-72-C-0328, March 1974.

17. Molusis, J.A., Hall, W.E., "Analysis of ACE Reentry Vehicle Aerodynamics by an Advanced System Identification Method," Final Report for ONR Contract No. N00014-75-C-0776, September 1975, Classified.

18. Mendel, J.M., "Postflight Data Analysis by Means of Adaptive, Iterated, Extended Kalman Filtering," IEEE AC-19, October 1974.

19. Mendel, J.M., "On Maximum Likelihood Estimation and Its Applicability to Postflight Data Processing," McDonnell Douglas Report No. MDC G5528, December 1974.

20. Chang, C.B., Whiting, R.H., Athans, M., "On the State and Parameter Estimation for Maneuvering Reentry Vehicles," IEEE AC, February 1977.

21. Graham, R.J., "Determination and Analysis of Numerical Smoothing Weights," NASA TR R-179, December 1968.

22. Belknap, S.B., of the Aerospace Corporation provided many useful inputs during the course of this work, mostly through private communications. The rate integration method for data reconstruction described in Chapter III is due to him.

23. Greville, T.N.E., Theory and Application of Spline Functions, Academic Press, New York, 1969.

24. Gupta, N.K., "Modeling of Nonlinear Systems Using Splines," Systems Control, Inc. Technical Memo, TM 5126-02.

25. Hocking, R.R., "Criteria for Selection of a Subset Regression: Which One Should Be Used?," Technometrics, November 1972.

26. Efroymson, M.A., Multiple Regression Analysis, in Mathematical Methods for Digital Computers, Ed. Ralston, A., and Wilff, M.S., Wiley, New York, 1962.

27. Furnival, G.M., Wilson, R.W., "Regression by Leaps and Bounds," Technometrics, November 1974.

28. The Aerospace Corporation, "Generalized Trajectory Simulation, Volume I: Overview," Report SAMSO-TR-75-255, Volume 1, November 1975.

29. Gupta, N.K, Hall, W.E. and Trankle, T.L., "Advanced Methods for Model Structure Determination from Test Data," AIAA Atmospheric Flight Mechanics Conference, AIAA Paper 77-1170, Hollywood, Florida, August 1977 (also to appear in the AIAA Guidance and Control Journal).

30. Gupta, N.K. and Mehra, R.K., "Computational Aspects of Maximum Likelihood Estimation and Reduction in Sensitivity Functions Computations," IEEE Transaction Auto. Control, Vol. AC-19, No. 6, pp. 774-783, December 1974.

31. Gupta, N.K. and Hall, W.E., "Design and Evaluation of Sensor Systems for State and Parameter Estimation," presented at AIAA Guidance and Control Conference, August 1977; also to appear in Journal of Guidance and Control.